JOURNAL OF PETROLOGY | VOLUME 42 | NUMBER 8 | PAGES 1471–1490 | 2001

Crystallization Driven by Decompression and Water Loss at Stromboli Volcano (Aeolian Islands, Italy)

NICOLE MÉTRICH[1]*, ANTONELLA BERTAGNINI[2], PATRIZIA LANDI[2] AND MAURO ROSI[3]

[1]LABORATOIRE PIERRE SÜE, CEA-CNRS, CE-SACLAY, 91191 GIF SUR YVETTE, FRANCE

[2]ISTITUTO NAZIONALE DI GEOFISICA, c/o DIPARTIMENTO DI SCIENZE DELLA TERRA, UNIVERSITÀ DEGLI STUDI DI PISA, VIA S. MARIA, 53, 56126 PISA, ITALY

[3]DIPARTIMENTO DI SCIENZE DELLA TERRA, UNIVERSITÀ DEGLI STUDI DI PISA, VIA S. MARIA, 53, 56126 PISA, ITALY

RECEIVED JULY 14, 2000; REVISED TYPESCRIPT ACCEPTED FEBRUARY 6, 2001

Stromboli, in the Aeolian Archipelago, is famous for its persistent volcanic activity. The 'normal' activity, consisting of rhythmic explosions ejecting crystal-rich scoriae, is periodically interspersed with more energetic explosions during which, in addition to crystal-rich scoriae, crystal-poor pumices are also emitted. The scoriae contain ~50 vol. % crystals (Plag ~65; Cpx ~25; Ol ~10) whereas the pumices display <10 vol. % crystals (Plag ~42–50; Cpx ~47–30; Ol ~11–20). The bulk rocks, mainly ranging between K-rich basalts and shoshonitic basalts, surprisingly exhibit only slight variations in major and trace element contents, and rare earth element patterns. Systematic studies of melt inclusions (MI) and their host minerals were performed on three scoria–pumice pairs erupted together during the violent explosions. The MI cover a compositional range (CaO/Al_2O_3 = 0·99–0·29) far wider than that of the whole rocks (CaO/Al_2O_3 = 0·69–0·52) and attest to the presence of rather primitive melts not yet identified as erupted magmas. On the basis of MI analyses, the crystal-poor magmas contain between 2·3 and 2·8 wt % H_2O, 894–1689 ppm CO_2, 2250–1660 ppm S and 2030–1660 ppm Cl, with the S/Cl ratio close to unity. In contrast, the crystal-rich magma is extensively degassed. We propose that this degassed magma, which sustains the 'normal' activity, results from the crystallization of volatile-rich magmas within the cone itself, driven by decompression and H_2O exsolution at low pressure. The crystallization is accompanied by S and Cl fractionation into the gas phase, consistent with partition coefficients D_S and D_{Cl} between fluid and melt of 40 and 10, respectively. The most violent explosions appear to result from the uprising and emission of volatile-rich magma blobs.

KEY WORDS: *Stromboli; Strombolian activity; melt inclusions; mineral chemistry; volatiles*

INTRODUCTION

Stromboli is a volcanic island in the Aeolian Archipelago (Southern Italy) famous in the volcanological literature for its persistent state of activity. Recent chronostratigraphic studies indicate that this activity started after a period dated between the third and seventh centuries AD (Rosi *et al.*, 2000). The volcanic cone is broadly elliptical, with a NE elongation, and rises from a depth of ~2000 m to an elevation of 924 m above sea level (a.s.l.). Eruptions occur from three main craters at 750 m a.s.l. in the Sciara del Fuoco, a horseshoe-shaped depression situated on the NW flank of the cone, produced by gravity collapses some 5–10 ky ago (Hornig-Kjarsgaard *et al.*, 1993; Pasquaré *et al.*, 1993; Kokelaar & Romagnoli, 1995). Eruptive activity is associated with a continuous streaming of gas from the crater area with an estimated output of 6000–12 000 tons/day of H_2O, CO_2, SO_2 and minor HCl and HF (Allard *et al.*, 1994). The current activity of the volcano includes: (1) persistent explosive activity ('normal' activity); (2) episodes of lava flow emission; (3) violent explosive events. Persistent 'normal' activity consists of rhythmic explosions that occur at intervals of 10–20 min, throwing incandescent lumps of lava, scoriae

Extended dataset can be found at http://www.petrology.oupjournals.org

*Corresponding author. Telephone: 33-1-69-08-85-11. Fax: 33-1-69-08-69-23. E-mail: metrich@drecam.cea.fr

Published by Oxford University Press 2001

and ash to heights of a few hundred metres. Most of the coarse ejecta fall back into the craters although some are expelled up to 200 m from the source vent. Explosions are generated by the violent expansion of large gas bubbles that rise at rather constant time intervals through glowing lava, which occupies the bottom of the craters. The ejected materials during normal activity are dark in colour, have low vesicularity and are rich in millimetre-sized crystals of plagioclase, pyroxene and olivine.

Every 10–20 years in the past two centuries the volcano has produced outpouring of lavas either from the summit craters or from fissures radiating from them, which have flowed onto the Sciara del Fuoco slope, eventually reaching the sea. Effusive episodes usually last from days to months. Lavas are also very porphyritic with phenocryst content and mineralogy similar to the products of the 'normal' activity.

The third type of activity consists of sudden major explosions and paroxysms (Barberi *et al.*, 1993). Major explosions result in blasts lasting tenths of seconds to minutes, which cause the ballistic fallout of metre-sized bombs and blocks up to several hundred metres from the craters, as well as scattered showers of lapilli and ash as far as the coast. An average of three major explosions per year have occurred over the past 6 years (Bertagnini *et al.*, 1999). Paroxysms represent the most violent eruptive manifestations of the volcano and can last from minutes to hours. During these events showers of incandescent scoriae and bombs fall out up to a distance of a few kilometres from the craters, sometimes affecting the two villages on the coast. As a result of their larger volume, paroxysms can lead to the accumulation of discrete, centimetre-thick lapilli beds. A few paroxysm episodes have also ejected a substantial amount of old material (blocks and lithics) as well as a large volume of ash and vapour. These events are normally accompanied by significant morphological changes of the crater area and the formation of deep craters (Perret, 1913).

One of the important features of both major explosions and paroxysms highlighted by recent studies is the frequent emission of crystal-poor, gold-coloured, highly vesicular pumices together with crystal-rich rather dense scoriae and bombs identical to those of the ordinary activity (Bonaccorso *et al.*, 1996; Bertagnini *et al.*, 1999; Coltelli *et al.*, 1999; Francalanci *et al.*, 1999). Most of the existing geophysical studies and dynamic models of the Strombolian explosions are based on the 'normal' activity (Chouet *et al.*, 1974, 1997; Jaupart & Vergniolle, 1988; Giberti *et al.*, 1992; Ripepe *et al.*, 1993, 1996; Vergniolle *et al.*, 1996). However, the major explosions and paroxysms may represent a key for understanding the origin of the persistent activity at Stromboli.

The aim of this paper is to shed new light on the behaviour of the magmatic plumbing system of the volcano by investigating the petrogenetic and physical relationships between the different types of magma which are emitted as highly vesicular pumices and crystal-rich black scoriae. We propose a general model of crystallization driven by decompression and water loss at the origin of the crystal-rich magma on the basis of the major and trace element geochemistry of bulk rocks, their mineralogy and a detailed study of olivine-hosted melt inclusions (MI).

ANALYSED MATERIAL

The studied samples consist of dense crystal-rich scoriae and highly vesicular pumices emitted during the 23 August 1998 major explosion and the last cycle of activity, which started after a period dated between the third and seventh centuries AD (Rosi *et al.*, 2000). Scoriae and pumices of 23 August 1998 were recovered on 24 August from the upper part of the cone within 0·5 km of the source vents. The other samples were collected from tephra beds in stratigraphic trenches dug on the NE flank of the cone at an elevation of ~500 m (Fig. 1). The age of the tephra succession and its relationship to the current activity of the volcano have been discussed by Rosi *et al.* (2000).

Chemical analyses of bulk rocks were obtained for 11 samples collected from the trenches (Fig. 1) and two scoria–pumice pairs from the 23 August 1998 explosion. Most of the samples from the trenches are pumices, which always incorporate fragments of crystal-rich scoriae, indicative of syn-eruptive mingling phenomena. Owing to the rare occurrence and small size of the scoriae, only two tephra beds in trench 2 allowed the analysis of individual pumice and scoria clasts (ST79s/p and ST82s/p, Fig. 1). Virtually unmingled crystal-poor pumices and crystal-rich scoriae exist among the products emplaced around the vents during the 23 August 1998 explosion and they are considered pure end-members. Mineral chemistry and melt inclusion studies were made on the unmingled pumice–scoria pairs from trench 2 (samples ST79s/p and ST82s/p) and from the 23 August 1998 explosion (samples ST130p and ST133s). A total of 148 melt inclusions (MI) were analysed, mainly hosted in olivine (120) and clinopyroxene (28) grains separated from 2 mm to 1/4 mm grain sizes.

EXPERIMENTAL PROCEDURES

Microanalyses of melt inclusions and groundmass glasses

Major elements, Cl, S and F of MI and groundmass glasses were determined using an SX50 CAMECA electron microprobe (Service Camparis, Paris VI). The analytical conditions were 10 nA beam current, 10 μm beam

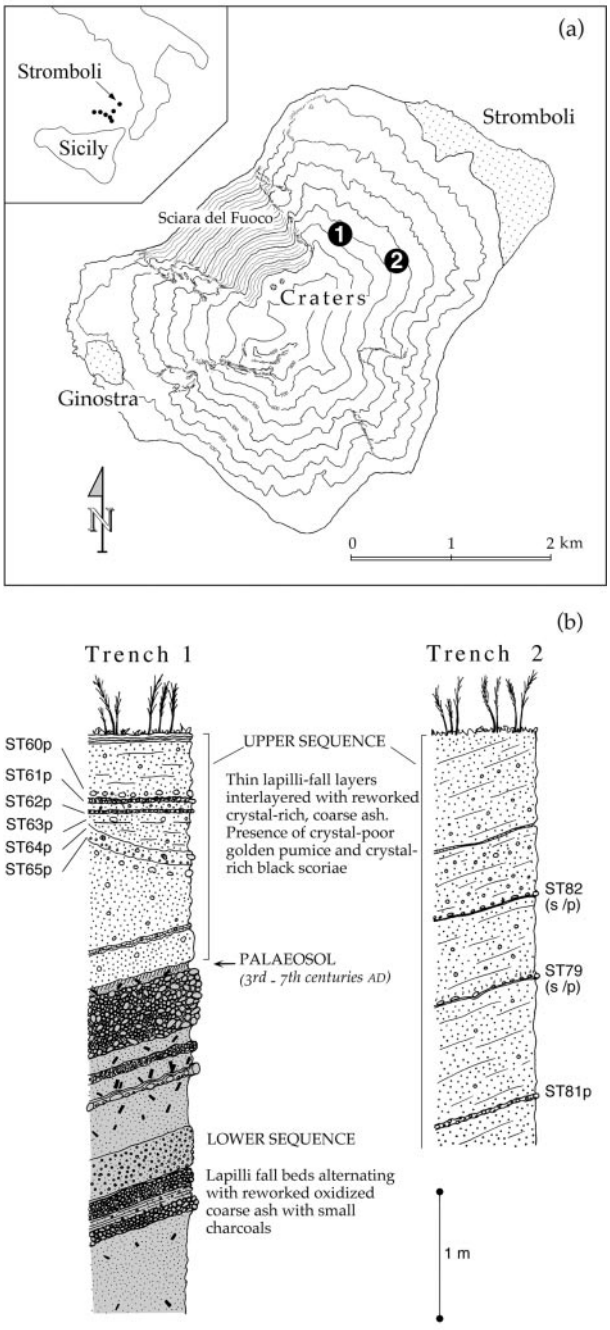

Fig. 1. (a) Topographic sketch of Stromboli island and location of trench 1 and trench 2. (b): Stratigraphic sections of trench 1 and trench 2 and location of analysed samples (p, pumice; s, scoria).

size and 10–15 s counting times for major elements, and 40 nA, 15 μm and 120 s for Cl, S and P. Reproducibility and accuracy of analyses were checked for S and Cl on Alv981 (S = 1110 ± 110 ppm; Métrich & Clocchiatti, 1996) and VG2 (Cl = 300 ± 35 ppm; S = 1450 ± 30 ppm) reference basaltic glasses. The international glass standard VG2 was previously found to contain 291–316 ppm Cl and 1348–1365 ppm S (Thordardson *et al.*, 1996). The shift of the S kα wavelength as a function of the oxidation state of sulphur was taken into account for S analysis as described by Métrich & Clocchiatti (1996). Fluorine was specifically analysed in scanning mode at 10 kV and 80 nA, with 200 s counting time, using silicic glass standards VNM50 and CFA47, containing 940 and 2000 ppm F, respectively (Mosbah *et al.*, 1991).

Carbon and water in double-faced polished MI were analysed by transmission IR spectroscopy using a Nicolet Magna-IR 550 spectrometer, equipped with a Globar source, an MCT/A detector cooled with N_2 and a KBr–XT beam splitter, and coupled with a Spectra-Tech microscope (Pierre Süe Laboratory, Saclay). Concentrations (C) were calculated according to the Beer–Lambert law: $C = 100AM/[\varepsilon\rho e]$, where A is the absorbance, M the molar mass (g/mol), ε the molar absorptivity (L/mol per cm), ρ the glass density, and e the thickness (cm). The doubly polished sample thickness is measured with an error of ±2–3 μm, using a Mitutoyo digital comparator. The average density, determined by the Archimedes method using distilled water, was 2·69 ± 0·02 g/cm^3 (13 measurements) on basaltic glass fragments containing from 2·5 to 3·5 wt % H_2O.

Water is dissolved as molecular water ($H_2O_{mol.}$) and hydroxyl groups (OH^-) in the MI. The concentrations of total water ($H_2O_{mol.} + OH^-$) in MI were determined using the broad band at 3535 cm^{-1} and/or by adding the concentrations of water dissolved in MI as molecular water and hydroxyl groups using the 5200 and 4500 cm^{-1} absorption bands, respectively. The peak heights were measured graphically relative to drawn linear baselines for the 3535, 4500 and 5200 cm^{-1} bands. The absorption coefficient ε^{3535} was determined to be 64·3 L/mol per cm by linear regression from basaltic glasses (MgO ~5·5 wt %, K_2O ~1·9 wt %) containing 1·2, 1·47, 3·1 and 3·5 wt % H_2O whose concentrations were determined by the Karl–Fisher titration (CRSCM-CNRS, Orléans). Comparable values of ε^{3535} were previously used for basaltic glasses (61 ± 1 L/mol per cm, Pandya *et al.*, 1992; 63 ± 3 L/mol per cm; Dixon *et al.*, 1995). The absorption coefficients ε^{5200} [$\varepsilon^{5200} = -2{\cdot}6 + 5{\cdot}1T$, where T = (Si + Al)/Σcations] and ε^{4500} ($\varepsilon^{4500} = -2{\cdot}3 + 4{\cdot}4T$) were calculated according to Dixon *et al.* (1995), and checked against the water-bearing glass fragments.

Carbon dissolved in MI is present as carbonate ions. Its concentration was determined in MI by measuring the peak height at 1515 cm^{-1} on the background-subtracted spectra as presented by Dixon *et al.* (1995), and after deconvolution taking into account the contribution of the molecular H_2O peak at 1630 cm^{-1}. The absorption coefficient at 1515 cm^{-1} (ε^{1515}) was calculated using the equation $\varepsilon^{1515} = 451 - 342[Na/(Ca + Na)]$, according to Dixon & Pan (1995). The C measurements were cross-checked against a C, H_2O-bearing basaltic glass

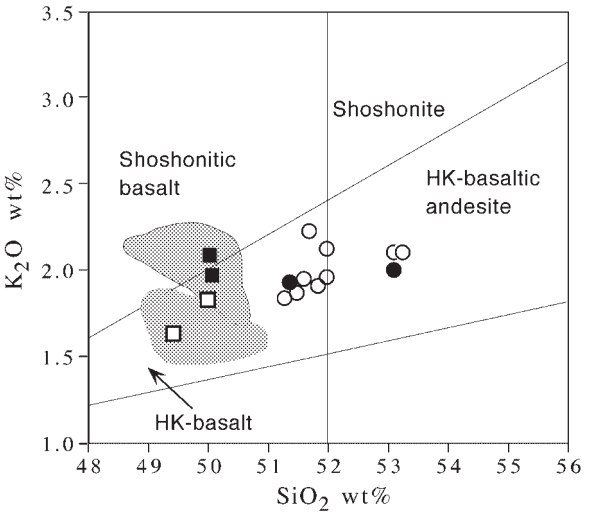

Fig. 2. Whole-rock compositions of samples from trenches and the 23 August 1998 explosion plotted in a SiO_2–K_2O classification diagram [modified after Peccerillo & Taylor (1976)]. The composition fields of pumice (light grey) and scoriae (dark grey) emitted in the past 15 years are shown. ○, pumice from the trenches; ●, scoriae from the trenches; □, pumice from the 23 August 1998 explosion; ■, scoriae from the 23 August 1998 explosion.

determined to contain 301 ppm C by Fourier Transform Infrared Spectroscopy (FTIR) (21 measurements, SD = 28) and 296 ± 45 ppm C by nuclear reaction $^{12}C(d, p)^{13}C$ using a nuclear microprobe (Métrich & Mosbah, 1988).

Optical thermometry

The temperatures of homogenization (T_h) of olivine-hosted MI were measured using double-faced polished olivine grains placed in the heating stage (Pierre Süe Laboratory, Saclay) purged with purified He as the carrier gas (Sobolev *et al.*, 1980). The temperatures were measured with a $Pt–Pt_{90}Rh_{10}$ thermocouple, and calibrated against the melting points of Ag (961°C) and Au (1063°C). The error on measurements is ~15°C.

GEOCHEMISTRY

Whole-rock compositions of the selected samples are reported in Table 1. All the scoriae and pumices from trenches belong to the K-rich magma series and range between HK-basalts and HK-basaltic andesites (SiO_2 ~51–53 wt %; K_2O ~1·8–2·2 wt %, Fig. 2). The 23 August 1998 samples are HK-basalts and shoshonitic basalts (SiO_2 ~49–50 wt %), similar to those erupted within the last 15 years (Fig. 2).

As a whole, the analysed clasts exhibit only slight variations in major, trace element and rare earth element (REE) profiles (Fig. 3, Table 1). They are characterized by light REE (LREE) enrichment (La/Yb from 18 to 23·9) and a slight negative anomaly in Eu indicative of plagioclase crystallization (Fig. 3a and b). Crystal-poor pumices may appear slightly less evolved than the crystal-rich scoriae, although the differences in MgO wt %, lithophile elements and LREE are at the limit of analytical error (Table 1, Fig. 3b). Thus, despite a large difference in amount of crystals the pumice–scoria pairs display only minor chemical variability.

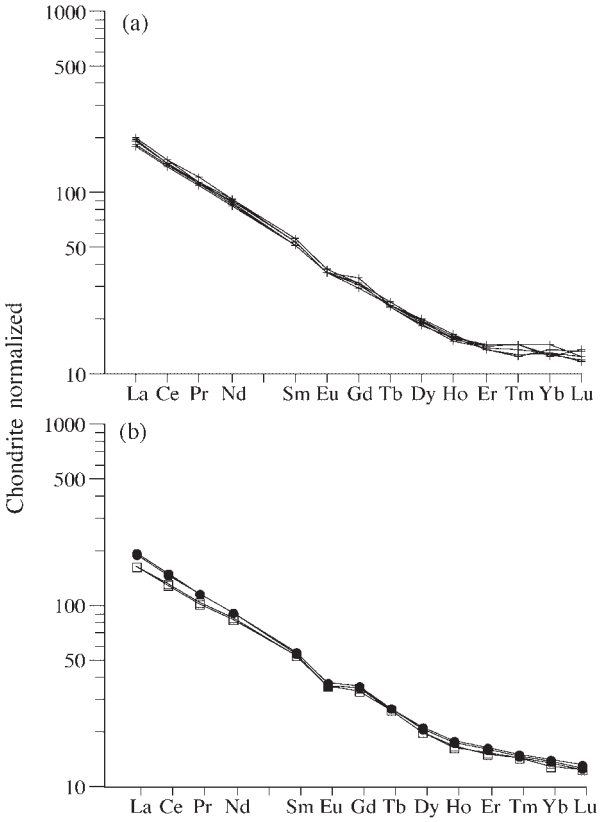

Fig. 3. (a) Chondrite-normalized REE patterns (McDonough & Sun, 1995) for selected samples from trenches (ST63, ST65, ST79s/p, ST82s/p). (b) Chondrite-normalized REE patterns (McDonough & Sun, 1995) for pumice–scoria pairs from 23 August 1998 explosion (●, scoria; □, pumice).

PETROGRAPHY AND MINERAL CHEMISTRY

Both pumices and scoriae are porphyritic with phenocrysts of plagioclase, clinopyroxene and olivine in a glassy matrix. On the basis of modal analyses, the scoriae contain ~50 vol. % crystals (Plag ~65; Cpx ~25; Ol ~10). The crystal content of the pumices is nearly 10–12 vol. % (Plag ~42–50; Cpx ~47–30; Ol ~11–20), but, as will be discussed further, this amount is an overestimate

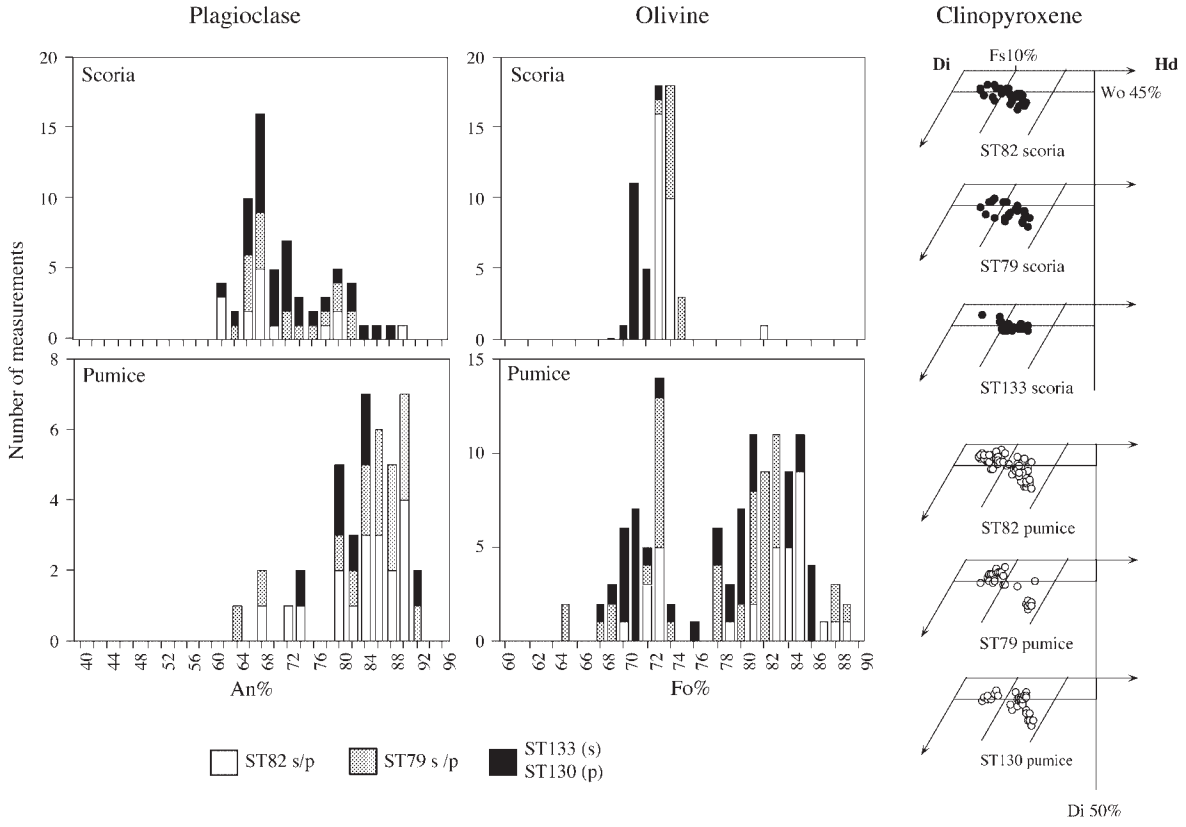

Fig. 4. Mineral compositions of pumice–scoria pairs from the trenches (ST79s/p; ST82s/p) and 23 August 1998 explosion (ST130p and ST133s). Plagioclase and olivine compositions represented as An mol % and Fo mol %, and clinopyroxene compositions represented in terms of the pyroxene quadrilateral. Analyses were carried out with a Philips XL30 scanning electron microscope equipped with EDAX X-4I at Dipartimento di Scienze della Terra di Pisa.

of the primary crystal content as most of the crystals are not in equilibrium. Pumices and scoriae also differ with respect to their groundmass, which is honey coloured and highly vesicular in the pumices and brown and less vesicular in the scoriae.

In scoriae, plagioclase compositions vary from An_{62} to An_{72} and show both dusty bands and sieve-textured resorbed cores with more calcic composition ($An_{74–90}$) (Fig. 4). Olivines exhibit narrow compositional ranges: $Fo_{70–73}$ in ST133s, $Fo_{73–74}$ in ST82s and $Fo_{73–75}$ in ST79s (Fig. 4). Clinopyroxene occurs both as euhedral, virtually homogeneous crystals ($Fs_{12–14}Wo_{42–45}$) in equilibrium with the glassy matrix and as zoned crystals with resorbed and patchily zoned cores ($Fs_{6–11}Wo_{45–47}$) surrounded by broad rims with the same composition as the homogeneous crystals. The inner patchy zones of the clinopyroxene of ST79s commonly have more evolved compositions ($Fs_{15–17}Wo_{43–40·5}$).

In pumices, plagioclase is calcic and ranges between An_{80} and An_{92}, although a few crystals have $An_{64–74}$ resorbed cores. Olivine exhibits also a wide range of composition from Fo_{70} to Fo_{89} (Fig. 4). Compositions of crystal rims in equilibrium with the glassy matrix are slightly variable from one sample to another: $Fo_{84–86}$ in ST130p, $Fo_{83–85}$ in ST82p and $Fo_{82–83}$ in ST79p. Euhedral or skeletal homogeneous crystals, in equilibrium, are rather rare in samples ST79p and ST82p (Fig. 5a) from trenches and were not found in the 23 August 1998 pumices (ST130p). In addition, a few crystals more magnesian than the olivines in equilibrium with the pumice glasses are found in ST79p (oln30, oln8) and ST82p (ol11; Fig. 5b). The crystals (oln8 and ol11) are homogeneous (Fo_{89} and $Fo_{87–88}$, respectively), whereas oln30 shows reverse zoning ($Fo_{88–86}$). In every sample, euhedral crystals with the composition of the olivine from scoriae ($Fo_{70–74}$) rimmed either by the glass of the scoriae or by a thin (<20 μm) $Fo_{82–86}$ rim in equilibrium with pumice are common (Fig. 5c). These are regarded as crystals of the crystal-rich magma admixed into the crystal-poor magma immediately before or during the eruption. Iron-rich olivines ($Fo_{65–68}$) with $Fo_{82–86}$ rims occur only in pumices ST79p. Many euhedral crystals show a strongly resorbed core ($Fo_{68–74}$), a large intermediate zone with highly variable composition between

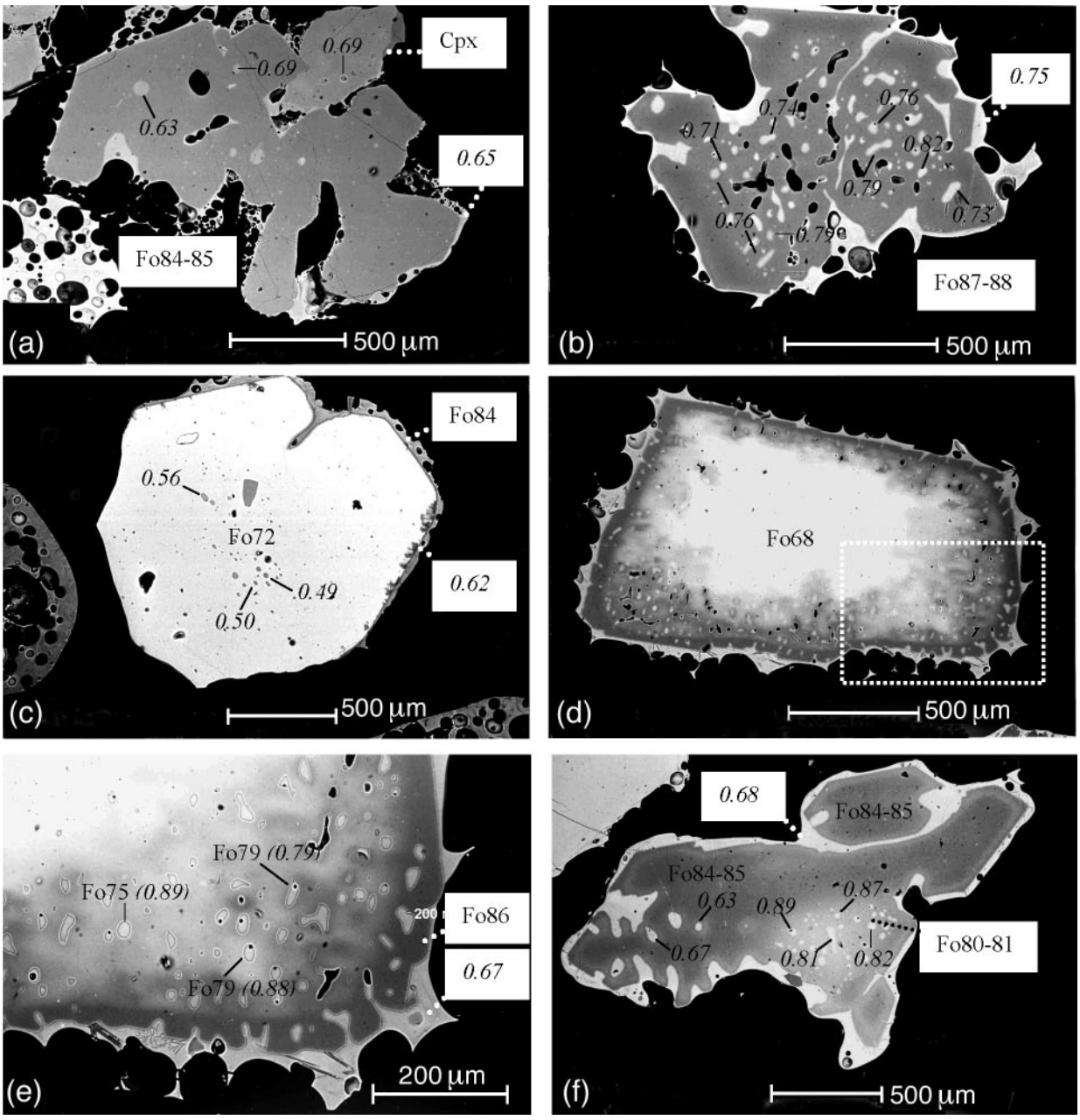

Fig. 5. Back-scattered electron micrographs of olivines from pumice. (a) Homogeneous crystal (ol4 in ST82p); the clinopyroxene in equilibrium with the olivine has a composition Fs_8Wo_{46}; (b) primitive olivine wetted by glass less evolved than the groundmass of the pumice (ol11 in ST82p); (c) homogeneous olivine Fo_{72} inherited from crystal-rich magma, with a thin (<20 μm) rim Fo_{84} in equilibrium with the groundmass of the pumice (ol3 in ST130p); (d) evolved olivine with a large reaction zone rich in MI, with a 50–70 μm outer rim Fo_{86} in equilibrium with the groundmass of the pumice (ol12 in ST130p); (e) enlargement of the reaction zone of olivine of (d). The distribution of MI together with the variable compositions of both MI and host olivine indicate the rapid growth of the crystal in disequilibrium conditions. (f) Olivine $Fo_{84–85}$ with skeletal rim and resorbed core $Fo_{80–81}$, rich in weakly evolved melt inclusions (ol8 in ST130p). Numbers in italics are CaO/Al_2O_3 of melt inclusions and rim glasses.

Fo_{71} and Fo_{86} and a magnesian outer rim ($Fo_{82–86}$) (Fig. 5d and e). Olivine, particularly in 23 August 1998 pumices, may also display skeletal structures with large homogeneous magnesian rims ($Fo_{84–86}$) and resorbed cores ($Fo_{73–80}$), rich in melt inclusions (Fig. 5f). Clinopyroxenes in equilibrium with the groundmass, present both as rims of zoned crystals and as small homogeneous crystals, are compositionally fairly uniform ($Fs_{5–8}Wo_{45–48}$). Zoned

Table 1: Representative chemical analyses of whole rocks (pumices and scoriae) from the trenches and the 23 August 1998 explosion

	Trench 1		Trench 2				23 August 1998 explosion			
	ST63p pumice	ST65p pumice	ST82s scoria	ST82p pumice	ST79s scoria	ST79p pumice	ST143s scoria	ST133s scoria	ST140p pumice	ST130p pumice
SiO_2	51·25	52·80	51·07	50·87	52·50	51·51	49·85	49·89	49·05	49·72
TiO_2	0·91	0·99	0·90	0·90	0·84	0·87	1·00	0·98	0·97	0·97
Al_2O_3	16·00	17·75	17·13	16·56	16·81	16·67	17·76	18·05	17·14	16·71
FeO	3·84	3·12	3·10	3·46	3·13	3·01	3·43	3·86	4·60	4·03
Fe_2O_3	4·94	5·27	5·18	5·11	4·76	5·10	5·43	4·90	4·40	4·95
MnO	0·16	0·15	0·16	0·16	0·15	0·15	0·17	0·16	0·16	0·17
MgO	6·55	4·67	6·58	6·66	6·07	6·34	6·24	5·97	6·93	6·62
CaO	10·84	9·22	10·59	10·91	9·91	10·34	10·83	10·78	11·59	11·46
Na_2O	2·52	2·74	2·42	2·39	2·42	2·75	2·47	2·60	2·38	2·53
K_2O	1·94	2·08	1·92	1·82	1·93	2·21	1·96	2·07	1·62	1·81
P_2O_5	0·38	0·38	0·39	0·40	0·37	0·39	0·45	0·45	0·42	0·45
H_2O	0·66	0·83	0·56	0·77	1·11	0·66	0·41	0·28	0·73	0·58
S_{total}	n.d.	n.d.	<0·01	0·037	n.d.	0·034	n.d.	<0·01	0·017	n.d.
CaO/Al_2O_3	0·68	0·52	0·62	0·66	0·59	0·62	0·61	0·60	0·68	0·69
K_2O/Na_2O	0·77	0·76	0·79	0·76	0·80	0·80	0·79	0·80	0·68	0·72
V	265	267	256	270	246	249	271	264	278	259
Cr	96	14	107	116	84	132	60	49	51	44
Co	33	28	31	34	30	31	33	33	34	33
Ni	47	20	44	51	46	49	44	41	46	43
Rb	65	72	65	62	66	73	68	66	52	53
Sr	751	668	716	742	687	756	733	734	701	700
Y	25	24	25	24	25	25	28	27	26	26
Zr	147	154	151	148	143	164	156	152	132	129
Nb	19	18	18	18	18	20	19	19	16	16
Mo	1·53	1·72	1·55	1·66	1·53	1·83	1·56	1·52	1·18	1·15
Cs	5·0	6·0	5·2	4·6	5·1	5·5	5·0	4·9	3·7	3·7
Ba	958	941	915	901	910	982	964	956	816	819
La	48	43	46	45	44	47	46	45	39	39
Ce	92	85	89	88	87	92	92	91	81	80
Pr	11·2	10·2	10·4	10·5	10·3	10·6	10·9	10·8	9·8	9·6
Nd	42	38	41	40	39·0	42	42	42	39	38
Sm	7·9	7·5	7·8	7·5	7·6	8·2	8·3	8·1	7·8	7·8
Eu	2·0	2·0	2·0	2·0	2·0	2·1	2·1	2·0	2·0	2·0
Gd	6·2	6·7	5·9	6·3	6·3	6·3	7·2	7·0	6·7	7·0
Tb	0·86	0·86	0·86	0·84	0·90	0·84	0·98	0·98	0·95	0·96
Dy	4·67	4·86	4·98	4·56	4·80	4·63	5·20	5·30	4·90	4·90
Ho	0·86	0·85	0·90	0·87	0·89	0·83	0·96	0·98	0·92	0·91
Er	2·32	2·28	2·18	2·19	2·27	2·24	2·60	2·65	2·44	2·46
Tm	0·36	0·36	0·31	0·32	0·36	0·34	0·37	0·38	0·36	0·36
Yb	2·00	2·34	2·18	2·11	2·04	2·07	2·25	2·26	2·10	2·17
Lu	0·34	0·31	0·33	0·29	0·30	0·31	0·32	0·33	0·31	0·31
Hf	3·4	3·5	3·5	3·1	3·4	3·4	3·7	3·6	3·2	3·2
Ta	1·18	1·15	1·14	1·07	1·05	1·22	1·11	1·09	0·90	0·92
Pb	18	18	17	16	16	18	17	17	14	16
Th	17·6	17·3	17·2	15·6	14·3	18·2	14·8	14·4	11·4	11·1
U	3·93	3·99	3·82	3·45	3·90	4·13	3·70	3·70	2·87	2·88

Major elements (from Rosi *et al.*, 2000) analysed by X-ray fluorescence, except for MgO, Na_2O and K_2O, analysed by atomic absorption spectrometry, and FeO, by titration. Trace elements were analysed by inductively coupled plasma emission (ICP-E) at Centre de Recherches Pétrographiques et Géochimiques (Nancy, France). Routine precision: 10–25% for concentrations <5 ppm; 5–10% for concentrations between 10 and 50 ppm; <5% for concentrations >50 ppm; n.d., not determined.

Table 2: Selected analyses of melt inclusions hosted in olivines, rim and groundmass glasses of pumices and scoriae

	23 August 1998 Pumices (ST130p)								Scoriae (ST133s)		
	ol8 MI-1	ol8 MI-2	ol8 emb.[a]	ol10 MI-1	ol2 MI-1	ol12 MI-4	ol12 rim glass	Gdm[b]	ol9 MI-1	ol10 MI-2	ol10 rim glass
SiO_2	46·78	45·97	47·71	51·66	47·32	45·06	48·18	49·07	52·34	51·74	52·07
TiO_2	1·07	1·03	1·06	1·35	1·05	0·98	1·09	0·98	1·77	1·51	1·53
Al_2O_3	16·39	15·93	17·26	13·63	15·64	14·21	16·84	16·91	16·38	15·48	16·12
FeO_{total}	9·29	10·12	8·43	10·91	11·94	14·48	8·84	8·36	9·22	10·97	9·65
MnO	0·26	0·16	0·11	0·24	0·12	0·36	0·14	0·22	0·17	0·29	0·2
MgO	4·62	4·60	4·83	3·21	2·82	3·74	4·96	5·73	1·62	3·26	3·4
CaO	12·77	13·01	11·72	6·86	12·72	12·60	11·25	10·88	8·47	6·96	7·66
Na_2O	2·18	2·08	2·67	3·12	2·28	2·00	2·57	2·63	3·44	3·47	3·4
K_2O	1·42	1·43	2·10	3·48	1·56	1·23	2·32	2·20	4·08	4·18	3·99
P_2O_5	0·77	0·71	0·69	0·91	0·71	0·54	0·73	0·76	0·88	1·08	1·3
S	0·171	0·181	0·114	0·065	0·068	0·108	0·030	0·009	0·036	0·071	0·007
Cl	0·177	0·172	0·139	0·168	0·132	0·106	0·118	0·109	0·102	0·184	0·105
Sum	95·91	95·40	96·83	95·60	96·35	95·40	97·06	97·85	98·52	99·19	99·43
CaO/Al_2O_3	0·78	0·82	0·68	0·50	0·81	0·89	0·67	0·64	0·52	0·45	0·48
K_2O/Na_2O	0·65	0·69	0·79	1·11	0·69	0·61	0·90	0·84	1·18	1·20	1·17
Host olivines[c]											
Fo mol %	83·6	81·4	83·9	71·1	80·4	75·4	86·0		71·5	72·0	71·6
SiO_2	39·97	39·12	39·69	37·87	39·23	38·37	40·25		38·26	38·13	38·23
MgO	43·94	42·68	44·44	35·48	41·89	38·43	45·81		35·6	36·12	35·68
FeO	15·39	17·39	15·22	25·77	18·24	22·39	13·25		25·26	25·02	25·27
MnO	0·45	0·48	0·37	0·58	0·26	0·47	0·39		0·52	0·5	0·47
CaO	0·25	0·33	0·28	0·3	0·39	0·34	0·3		0·36	0·24	0·35
X_{Fo}[d]	0·05	0·04	0·03	0·01	0·11	0·07			0·06	0·02	
Recalculated compositions[e]											
SiO_2	46·43	45·69	47·46	51·47	46·43	44·56			51·55	51·47	
TiO_2	1·01	0·99	1·02	1·33	0·94	0·90			1·67	1·48	
Al_2O_3	15·53	15·30	16·73	13·44	13·92	13·16			15·46	15·17	
FeO_{tot}	9·61	10·41	8·64	11·12	12·63	15·06			10·12	11·25	
MnO	0·24	0·15	0·11	0·23	0·10	0·34			0·16	0·28	
MgO	6·67	6·13	6·05	3·66	7·12	6·31			3·52	3·92	
CaO	12·12	12·51	11·36	6·77	11·36	11·70			8·02	6·82	
Na_2O	2·07	1·99	2·59	3·08	2·03	1·85			3·25	3·40	
K_2O	1·35	1·37	2·03	3·43	1·39	1·13			3·85	4·10	
P_2O_5	0·73	0·68	0·67	0·90	0·63	0·50			0·83	1·06	
S	0·162	0·173	0·110	0·064	0·061	0·100			0·034	0·069	
Cl	0·167	0·165	0·135	0·165	0·117	0·098			0·096	0·180	

crystals have resorbed, patchily zoned cores ($Fs_{10–17}Wo_{44–40}$) with the same compositional range shown by the clinopyroxenes of scoriae. Clinopyroxenes inherited from the crystal-rich magma, which exhibit thin magnesian rims (<20 μm) or are rimmed by the glass of the scoriae, are also common.

	Trenches Pumices (ST82p)									Scoriae (ST82s)		
	oln50 MI-a	oln52 MI-a,b,c	oln28 MI-a	oln9 MI-a,b,c	ol11 MI-1,2,3	ol11 rim glass	ol3[f] MI-1,2	ol3[f] MI-4	Gdm[b]	oln2 MI-1	oln4 MI-1	oln3 rim glass
SiO_2	49·47	47·76	46·57	47·35	47·78	51·61	53·30	51·24	48·97	52·94	51·22	52·23
TiO_2	0·89	0·98	1·22	0·99	0·81	0·90	1·73	1·77	0·95	1·46	n.d.	1·59
Al_2O_3	15·85	16·53	15·59	15·91	15·83	17·17	15·52	15·02	17·48	15·25	15·2	15·26
FeO_{total}	8·39	7·84	7·60	8·43	7·73	7·35	8·69	10·52	8·25	9·51	11·2	9·86
MnO	0·19	0·16	0·17	0·19	0·14		0·16	0·26	0·16	0·18	0·16	0·17
MgO	5·24	4·42	5·11	3·27	6·90	5·65	2·31	2·88	5·75	3·23	3·62	3·64
CaO	10·22	12·49	13·23	13·58	12·24	12·81	7·81	8·42	10·97	6·94	7·9	7·29
Na_2O	2·49	2·42	2·22	2·19	2·28	2·46	3·38	3·28	2·68	3·55	3·35	3·30
K_2O	2·01	1·73	1·66	1·54	1·61	2·04	4·00	3·44	2·15	3·87	3·24	3·90
P_2O_5	0·61	0·59	0·55	0·63	0·56		1·09	1·12	0·62	0·77	0·99	1·08
S	0·123	0·173	0·186	0·205	0·169		0·011	0·085	0·046	0·074	0·089	0·005
Cl	0·159	0·186	0·192	0·204	0·174		0·118	0·175	0·126	0·227	0·255	0·126
Sum	95·64	95·28	94·29	94·47	96·22	100·00	98·10	98·22	98·14	98·00	97·23	98·46
CaO/Al_2O_3	0·64	0·76	0·85	0·85	0·77	0·75	0·50	0·56	0·63	0·46	0·52	0·48
K_2O/Na_2O	0·81	0·71	0·75	0·70	0·71	0·83	1·18	1·05	0·80	1·09	0·97	1·18
Host olivines[c]												
Fo mol %	83·7	84·6	85·9	84·4	87·6	88·0	72·5	72·5		72·7	72·8	72·7
SiO_2	40·77	39·85	39·44	39·38	40·27	40·34	37·96	37·96		37·45	38·18	37·45
MgO	44·83	44·79	44·92	44·53	47·09	47·51	36·49	36·49		36·41	36·56	36·41
FeO	15·51	14·51	13·17	14·72	11·89	11·56	24·66	24·66		24·36	24·40	24·36
MnO	0·25	0·28	0·27	0·31	0·38	0·27	0·57	0·57		0·37	0·56	0·37
CaO	0·29	0·27	0·29	0·30	0·37	0·33	0·31	0·31		0·37	0·30	0·37
X_{Fo}[d]	0·02	0·04	0·04	0·09	0·02		0·03	0·03		0·01	0·01	
Recalculated compositions[e]												
SiO_2	49·29	47·43	46·32	46·67	47·60		52·88	50·84		52·85	51·04	
TiO_2	0·87	0·94	1·18	0·90	0·79		1·68	1·72		1·45		
Al_2O_3	15·54	15·84	15·05	14·55	15·44		15·10	14·57		15·16	14·99	
FeO_{tot}	8·53	8·12	7·79	8·96	7·83		9·12	10·95		9·60	11·38	
MnO	0·18	0·15	0·16	0··17	0·14		0·15	0·26		0·18	0·16	
MgO	6·03	6·11	6·51	6·78	7·88		3·23	3·89		3·43	4·08	
CaO	10·02	11·98	12·78	12·45	11·95		7·61	8·18		6·91	7·79	
Na_2O	2·44	2·32	2·14	2·00	2·23		3·29	3·18		3·53	3·30	
K_2O	1·97	1·65	1·60	1·41	1·57		3·89	3·33		3·84	3·19	
P_2O_5	0·59	0·57	0·53	0·58	0·55		1·06	1·09		0·76	0·98	
S	0·121	0·166	0·179	0·188	0·166		0·010	0·082		0·074	0·087	
Cl	0·155	0·178	0·185	0·187	0·171		0·114	0·169		0·226	0·251	

MELT INCLUSIONS

The MI analysed are mainly hosted in olivine. Because the MI in diopside are scarce and frequently devitrified, and Fe-rich clinopyroxenes often contain glass corresponding to residual liquids that invaded the crystals at a later stage, less effort was devoted to these MI. In plagioclases, MI are often too small to be analysed. Glass adhering to the crystals (rim glass) and groundmass glasses were also analysed. The representative compositions in major elements, Cl, S and F of MI, rim and groundmass glasses are reported in Tables 2 and 3. The entire dataset

Table 2: continued

	Pumices (ST79p)								Scoriae (ST79s)			
	oln8 MI-a	oln30 MI-a-d	oln30	oln30 mixing[g]	oln23 MI-a	ol in cpx MI-1[h]	oln14 MI-a,b,c	ol3[f] MI-2	ol9 MI-1,2,3	ol9 rim glass	n10S MI-a	n6S rim glass
SiO_2	47·34	47·74	50·10	49·55	50·15	48·93	50·05	56·55	49·70	51·11	51·89	51·49
TiO_2	0·86	0·91	0·88	0·88	0·87	1·15	0·88	1·30	0·88	0·87	1·45	1·33
Al_2O_3	14·78	15·76	17·31	17·89	18·15	17·24	18·10	14·21	17·20	17·61	15·58	15·91
FeO_{total}	8·50	6·43	5·81	7·47	7·48	8·34	6·80	9·74	8·59	7·86	10·08	9·26
MnO	0·13	0·13	0·12	0·24	0·25	0·13	0·13	0·16	0·19	0·19	0·27	0·20
MgO	5·12	4·36	4·18	3·95	3·50	2·45	2·16	2·23	3·82	5·17	3·41	3·96
CaO	14·42	15·23	11·65	10·35	10·83	11·19	10·69	4·91	10·62	9·85	7·73	7·78
Na_2O	2·18	2·42	2·70	3·28	3·01	2·74	3·06	2·91	2·56	2·96	3·25	3·33
K_2O	1·57	1·71	2·32	2·71	2·49	2·33	2·61	4·44	1·61	2·63	3·59	3·49
P_2O_5	0·55	0·57	0·57	0·60	0·648	0·58	0·63	0·70	0·47	0·61	1·03	0·93
S	0·224	0·239	0·211	0·114	0·167	0·158	0·138	0·018	0·161	0·044	0·007	0·007
Cl	0·203	0·216	0·191	0·172	0·186	0·193	0·187	0·271	0·164	0·116	0·121	0·125
Sum	95·88	95·72	96·03	97·21	97·73	95·42	95·44	97·44	95·97	99·03	98·41	97·81
CaO/Al_2O_3	0·98	0·97	0·67	0·58	0·60	0·65	0·59	0·35	0·62	0·56	0·50	0·49
K_2O/Na_2O	0·72	0·71	0·86	0·83	0·83	0·85	0·85	1·53	0·63	0·89	1·11	1·05
Host olivines[c]												
Fo mol %	89·0	88·0	88·0	86·4	84·7	81·8	82·3	68·3	81·9	82·3	72·8	72·4
SiO_2	40·47	40·41	40·24	40·33	39·91	39·75	39·45	37·26	39·49	39·53	37·86	37·43
MgO	47·79	47·42	46·60	45·60	44·57	42·68	42·72	33·84	42·96	43·28	36·26	35·93
FeO	10·19	11·49	11·33	12·83	14·34	16·89	16·33	28·01	16·92	16·62	24·13	24·37
MnO	0·27	0·12	0·35	0·15	0·28	0·33	0·20	0·60	0·43	0·39		0·62
CaO	0·29	0·35	0·29	0·29	0·33	0·35	0·26	0·29	0·20	0·18	0·29	0·28
X_{Fo}[d]	0·12	0·06	0·05	0·07	0·06	0·08	0·07	0·03	0·04		0·01	0·00
Recalculated compositions[e]												
SiO_2	46·51	47·31	49·65	48·91	49·50	48·20	49·36	56·07	49·34		51·75	
TiO_2	0·76	0·86	0·84	0·82	0·82	1·06	0·83	1·26	0·86		1·43	
Al_2O_3	13·01	14·84	16·54	16·63	17·00	15·86	16·92	13·86	16·74		15·43	
FeO_{tot}	8·70	6·73	6·05	7·84	7·91	9·02	7·42	10·20	8·70		10·22	
MnO	0·12	0·12	0·12	0·22	0·24	0·12	0·12	0·16	0·20		0·26	
MgO	10·24	6·89	6·09	6·87	6·09	5·67	4·79	3·02	5·32		3·74	
CaO	12·73	14·36	11·14	9·64	10·17	10·32	10·01	4·80	10·06		7·66	
Na_2O	1·92	2·28	2·57	3·05	2·82	2·52	2·86	2·83	2·60		3·22	
K_2O	1·38	1·61	2·21	2·52	2·33	2·14	2·44	4·33	1·84		3·56	
P_2O_5	0·48	0·54	0·54	0·56	0·61	0·54	0·59	0·68	0·511		1·02	
S	0·197	0·225	0·202	0·106	0·156	0·145	0·129	0·018	0·155		0·007	
Cl	0·179	0·203	0·182	0·159	0·174	0·177	0·175	0·264	0·17		0·120	

[a]Embayment: gulf in mineral. [b]Groundmass glass. [c]Host olivine composition 100 × [Mg/(Mg + Fe)]. [d]Fraction of olivine crystallized after entrapment. [e]Composition recalculated on the basis of $K_D = [(FeO/MgO)_{ol}/(FeO/MgO)_{melt}] = 0·29$, following Métrich & Clocchiatti (1996). [f]Olivine inherited from the crystal-rich magma with a thin rim ($Fo_{84–86}$). [g]Mixing between magmas of different compositions (see text). [h]MI in olivine itself trapped in a pyroxene ($Fs_{6·2}Wo_{46·7}$).

is available as an electronic appendix on the *Journal of Petrology* Web site, at:
http://www.petrology.oupjournals.org.

Major element composition

In 23 August 1998 pumices, the olivine crystals contain numerous and irregular MI whose size varies from 25 to 50 μm, which probably result from rapid crystal growth and melt trapping during decompression (Fig. 5f). Similar observations are also valid for the pumices from the trench (ST82p, ST79p), although euhedral crystals with primary MI well preserved as glass inclusions with one or two bubbles also exist. In some of the bubbles, crystals line the inner walls of the bubbles. Similar crystals were determined by Raman spectroscopy to be Mg-carbonates in other samples from either Stromboli (N. Métrich, unpublished data, 1999) or Mt Etna in Sicily (Métrich & Mosbah, 1988). They are interpreted as a post-trapping reaction between CO_2 ($\pm$ H_2O) in the gas bubble and the H_2O-rich silicate melt to form carbonates, and related to either CO_2 ($\pm$ H_2O) diffusion from silicate towards the gas bubble or heterogeneous trapping of silicate melt and the associated CO_2 ($\pm$ H_2O)-rich vapour. In the studied samples, the hypothesis of heterogeneous trapping is consistent with the variation of the volume ratio ($V_{bubble}/V_{inclusion}$) between the bubble and the inclusion (Roedder, 1984).

Olivine ($Fo_{70–74}$) from scoriae contains primary rounded MI, with one or no bubble. Their size varies from 25 to (rarely) 80 μm. In the Fe-rich olivines ($Fo_{65–68}$), MI may contain a small sulphide globule associated with the bubble, and Fe–Ti oxides.

The MI compositions in olivine were corrected for post-entrapment crystallization by adding olivine component whose composition is determined in the vicinity of the inclusion, to obtain olivine–liquid equilibrium with K_D $[(FeO/MgO)_{ol}/(FeO/MgO)_{melt}]$ = 0·29 for Stromboli melts, and $[Fe^{3+}/(Fe^{2+} + Fe^{3+})]$ = 0·2 (Métrich & Clocchiatti, 1996). The effect of post-entrapment crystallization of olivine on most of the MI compositions is limited and should not significantly affect the ratio between elements except for Fe and Mg (Table 2). In the discussion, only the major element and volatile concentrations corrected for post-entrapment olivine crystallization have been taken into account.

As a whole, MI compositions define a compositional trend (CaO/Al_2O_3 = 0·99–0·29) associated with variable host olivines ($Fo_{89–64}$; Fig. 6) far larger than the range exhibited by the whole rocks (CaO/Al_2O_3 = 0·69–0·52, Table 2). Most of the MI in olivine $Fo_{70–75}$ from scoriae display a narrow range of compositions (CaO/Al_2O_3 ~0·6–0·4) close to that of the groundmass (Fig. 6). The MI compositions in crystals of $Fo_{70–75}$ with thin $Fo_{84–86}$ rims, separated from pumice, overlap those of MI of scoriae (Figs 5c and 6), thus confirming the provenance of these crystals from the crystal-rich magma. The most evolved MI (CaO/Al_2O_3 = 0·29–0·35) in equilibrium with olivines ($Fo_{65–68}$) were observed in ST79p (Fig. 6).

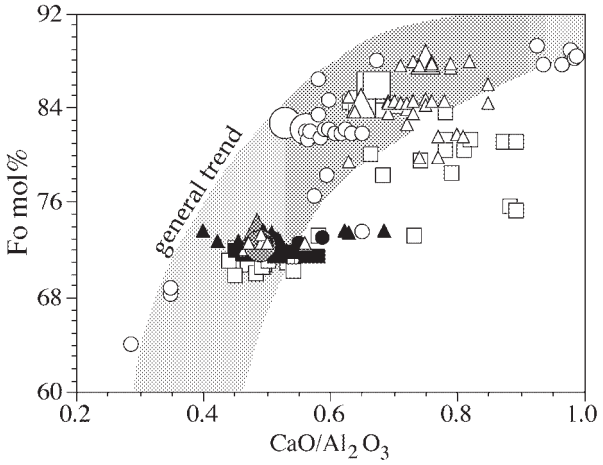

Fig. 6. CaO/Al_2O_3 of melt inclusions vs Fo [100Mg/(Mg + Fe)] content of host olivine in pumice–scoria pairs. Compositions of both groundmass glasses and rim glasses adhering to the crystal faces of olivines compared with the Fo content of the olivine outer rim are also plotted. The grey area shows a general evolutionary trend (see text). Circle, ST79; triangle, ST82; square, 23 August 1998 (ST130p, ST133s). Open symbols, pumice; filled symbols, scoria; large open symbols, groundmass and rim glass of pumice; large grey symbols, groundmass and rim glass of scoria.

Conversely, in pumices, they show highly variable compositions, which mirror the compositional variability of the crystals. The MI with CaO/Al_2O_3 ratios close to that of the groundmass of pumices are found only in olivine $Fo_{82–86}$ considered in equilibrium with the crystal-poor magma, and which occurs both as rare homogeneous crystals (Fig. 5a) and as the outer rims of zoned crystals (Fig. 5f). The olivines ($Fo_{87–89}$), present in the samples from the trenches only, contain the most primitive MI, which are less evolved than either the groundmass glasses or the bulk rocks. One crystal (ol11, ST82p sample) has preserved both MI and a very thin film of glass wetting the crystal with relatively high CaO/Al_2O_3 ratio (~0·75) indicative of the involvement of more primitive magma (Fig. 5b).

Several MI depart from the evolutionary trend in Fig. 6, showing a high CaO/Al_2O_3 ratio with respect to the composition of host mineral. They are found in both the large intermediate reaction zones and the resorbed cores of strongly zoned crystals, where they are particularly abundant and of small size, <25 μm (Fig. 5d–f). These features suggest crystallization and melt trapping out of equilibrium, probably during magma mingling and mixing events.

The MI compositions in diopsidic clinopyroxene were corrected on the basis of the CaO/Al_2O_3 ratio of MI in olivine in equilibrium with the clinopyroxene. The compositions of MI in clinopyroxenes $Fs_{12–14}Wo_{42–45}$ and $Fs_{6–8}Wo_{45–48}$ overlap those of the groundmass of the scoriae (CaO/Al_2O_3 = 0·37–0·48) and pumices (CaO/Al_2O_3 = 0·63–0·70), respectively. Some more evolved compositions (CaO/Al_2O_3 = 0·29) are found in Fe-rich clinopyroxenes $Fs_{15–18}Wo_{43–40·5}$.

Despite disequilibrium phenomena, all the MI in clinopyroxenes and olivines, together with groundmass glasses, define chemical trends that are characterized by rather abrupt changes for CaO/Al_2O_3 close to 0·6 (Fig. 7). The K_2O content in MI slightly varies (1·2–1·6 wt %) for CaO/Al_2O_3 ratio >0·6 and rapidly increases in the most evolved glasses up to 6 wt %. The Al_2O_3 concentration increases in the interval CaO/Al_2O_3 = 0·90–0·60 and then decreases for CaO/Al_2O_3 <0·6. Only the less evolved MI (CaO/Al_2O_3 >0·90), in ST79p olivine, depart slightly from the general trends mainly at higher contents of K_2O.

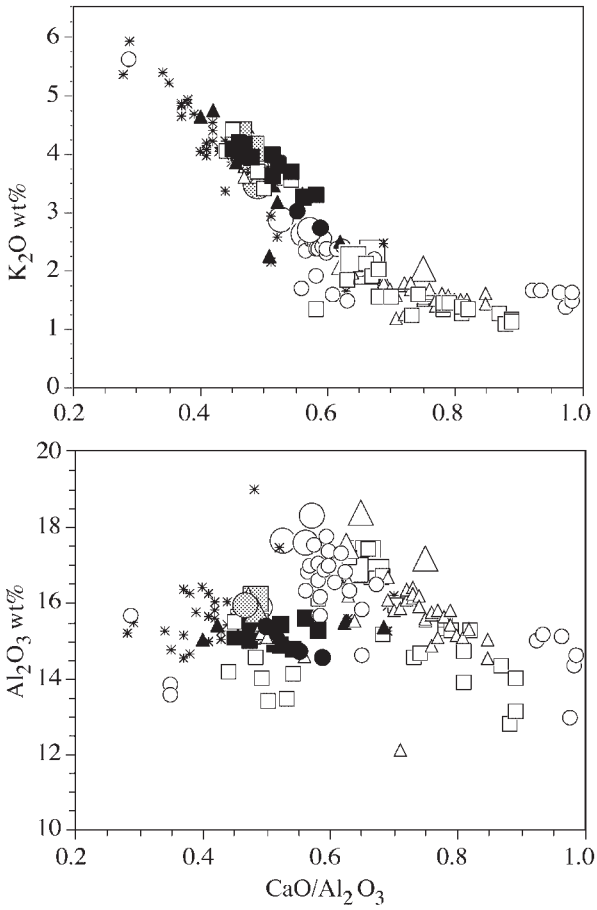

Fig. 7. Melt inclusion compositions in CaO/Al_2O_3 vs Al_2O_3 and K_2O diagrams. *, MI in clinopyroxenes; other symbols as in Fig. 6.

Volatile elements

As a whole, there is a general decrease in S and Cl concentrations in the MI from the more basic to the most evolved compositions (Fig. 8a and b).

In pumices (ST130p, ST82p), MI (K_2O = 1·4–1·6 wt %) in olivine ($Fo_{88–85}$) contain on average 1660 ± 100 ppm S, from 1730 to 1660 ± 100 ppm Cl (Fig. 8c and d) and from 640 to 680 ± 120 ppm F (Table 3). Between the samples, the differences measured in S, Cl and F content of MI are limited, and the S/Cl and Cl/F ratios are 0·95–1·0 and 2·7–2·4, respectively. The MI inclusions in clinopyroxenes indicate similar results. In the ST79 pumices, the highest values for both S (2250–1970 ppm) and Cl (2030–1790 ppm) are recorded in the MI (CaO/Al_2O_3 = 0·93–0·98; Fig. 8a and b) in olivine Fo_{88}, although the S/Cl ratio is also close to unity. The MI with CaO/Al_2O_3 ratio between 0·56 and 0·62 have 1560–1060 ppm S and from 1740 to 1590 ppm Cl (Fig. 8a and b). Two MI were measured to contain 703 and 868 ppm F (Table 3).

In scoriae, the MI display sulphur contents from 880–620 ppm to 190 ppm, significantly lower than those in MI from pumices (Fig. 8a and c), and highly variable Cl concentrations (2540–1020 ppm; Fig. 8b and d). The F concentrations are measured from 1157 to 1260 ppm (ST133s MI), and from 958 to 1364 ppm F (ST82s MI), the Cl/F ratio ranging from 1·4 to 2·5 (Table 3). It is worth noting that olivine crystals ($Fo_{70–74}$) inherited from the crystal-rich magma (scoriae), separated from pumice clasts, have trapped extensively degassed residual melts (CaO/Al_2O_3 ~0·50; 100 ppm S; 1290–1140 ppm Cl; Fig. 5c). The presence of a thin outer rim ($Fo_{84–86}$) in equilibrium with pumice glass indicates that S and Cl loss, as recorded by MI, occurred before the eruption, by degassing. In addition, the measurements of highly dispersed concentrations of S and Cl in MI trapped within the same olivine ($Fo_{80–73}$; e.g. ST130p-ol13; 1620–170 ppm S) also indicate the occurrence of degassing together with mixing between magmas with highly variable volatile contents, as will be discussed below.

Commonly, the groundmass glasses in both pumices and scoriae display comparable concentrations in Cl (from 1260 to 1030 ± 70 ppm) and S (~80 ppm, the minimum detection limit), whereas the F concentrations may differ from 776 ppm F (pumice ST130p) to 1046 ppm F (scoria ST133s). However, we also analysed rim glasses and embayments (gulfs) within the crystals from the pumices, which have recorded a rather large range of S concentrations from 1120 to ~80 ppm. This is well illustrated in the 23 August 1998 pumices (Fig. 8a and c) and reflects the relative efficiency of the syn-eruptive

Table 3: Fluorine, Cl, K_2O concentrations of rim glasses and melt inclusions in olivine

Sample		K_2O (wt %)	Cl (wt %)	F (ppm)	Cl/F
St130p					
ol8	emb.	2·03	0·135	654	2·1
ol8	rim gl.	1·98	0·139	846	1·6
ol13	rim gl.	1·99	0·130	775	1·7
ol13	rim gl.	1·99	0·130	734	1·8
ol9-1	MI	4·42	0·117	1046	1·1
ol6-1	MI	4·13	0·141	1172	1·2
ol13-1	MI	1·62	0·167	673	2·5
ol13-2	MI	1·55	0·134	687	1·9
ST133s					
ol10-1	MI	3·95	0·254	1261	2·0
ol10-2	MI	4·10	0·180	1252	1·4
ol10-3	MI	4·18	0·198	1157	1·7
ol9	rim gl.	4·34	0·103	1059	
ol9	rim gl.	4·34	0·103	1093	
ol9	rim gl.	4·34	0·103	986	
average		4·34	0·103	1046	1·0
St79s					
ol9-1,2,3	MI	1·84	0·167	703	2·4
oln10S-a	MI	3·56	0·120	868	1·4
St82s					
ol2-1	MI	1·70	0·155	641	2·4
ol11-1	MI	4·65	0·238	958	2·5
ol12-1	MI	2·24	0·201	1364	1·5
ol12-2	MI	2·04	0·228	1361	1·7

The F concentrations are corrected for the post-entrapment crystallization of olivine (see text). emb., embayment (gulf); gl., glass; MI, melt inclusions.

degassing at the time of eruption. Probably, the sulphur concentrations are closely linked with the vesicularity of pumice clasts.

Carbon and water contents in the MI were determined in scoriae and pumices from ST82 and ST79 only (Table 4a and b). The rather low number of analyses is explained by the very small size of the MI, which makes their preparation for FTIR very difficult.

All the analyses performed on the most evolved MI in olivines from scoriae indicate extensively degassed glasses with very low H_2O concentrations comparable with those of groundmass glasses (0·2 wt %; Table 4a). Their CO_2 contents are below the 40–50 ppm detection limits. The concentrations in CO_2 and H_2O range from 1689 to 894 ppm and from 2·8 to 2·3 wt %, respectively, in MI in olivines from pumices (Table 4b). The CO_2 concentrations decline with decreasing CaO/Al_2O_3 ratio (Fig. 9b) and increasing H_2O concentrations (Fig. 9c). Carbonate crystals in bubble are observed in MI with the highest CO_2 concentrations (1689 ppm CO_2, ST82p n9; Fig. 9a) confirming heterogeneous trapping and thus magma saturation with respect to CO_2-rich vapour phase at time of entrapment. The relatively low CO_2 concentration (1106 ppm) measured in MI (ST79p sample) with high CaO/Al_2O_3 ratio ($\sim$1·0) and trapped in olivine (Fo_{88}) with outer rim (Fo_{86}) also supports trapping from magmas heterogeneous with respect to their dissolved volatile content together with the relative proportions between the silicate melt and the gas phase. On the other hand, the MI are preserved as glassy inclusions and the post-entrapment evolution appears to be limited, suggesting that the possible H_2O loss after trapping, as described for fluid inclusions in olivine (Pasteris, 1987), should not be significant.

Some intermediate H_2O values, between 2·4–2·8 and 0·2 wt %, should exist but they may not have been analysed because of the small size of inclusions, which often reveal crystallization out of equilibrium and trapping from strongly heterogeneous magmas.

Optical thermometry

Heating stage experiments were performed on olivine-hosted MI from the ST82p/s pairs. During heating, MI became opaque because of nucleation, which occurs below 600°C in H_2O-rich MI (ST82p) and at $\sim$800°C in H_2O-poor MI (ST82s). The kinetics of crystal nucleation and melting are faster in H_2O-rich MI from pumice samples than in the others. The temperature of melting (T_m) of these nuclei (Roedder, 1984) was determined to lie between 1085 and 1105°C, with a mean value of 1090 $\pm$ 15°C (seven measurements) in H_2O-rich MI and from 1090 to 1102 $\pm$ 15°C with a mean value of 1098 $\pm$ 15°C (nine measurements) in H_2O-poor MI (Table 5).

Temperatures of homogenization (T_h) are obtained, after short experiments, when the bubble disappears. Most of the MI from pumice samples do not homogenize because of heterogeneous trapping and variable bubble/inclusion volume ratio, as described above. When the homogenization is obtained, we have checked that several inclusions within the same grain homogenized at the same temperature, in every set of samples. The T_h determined on MI from different crystals are 1125 and 1140 $\pm$ 15°C (ST82p) and 1100, 1115 and 1125 $\pm$ 15°C (ST82s).

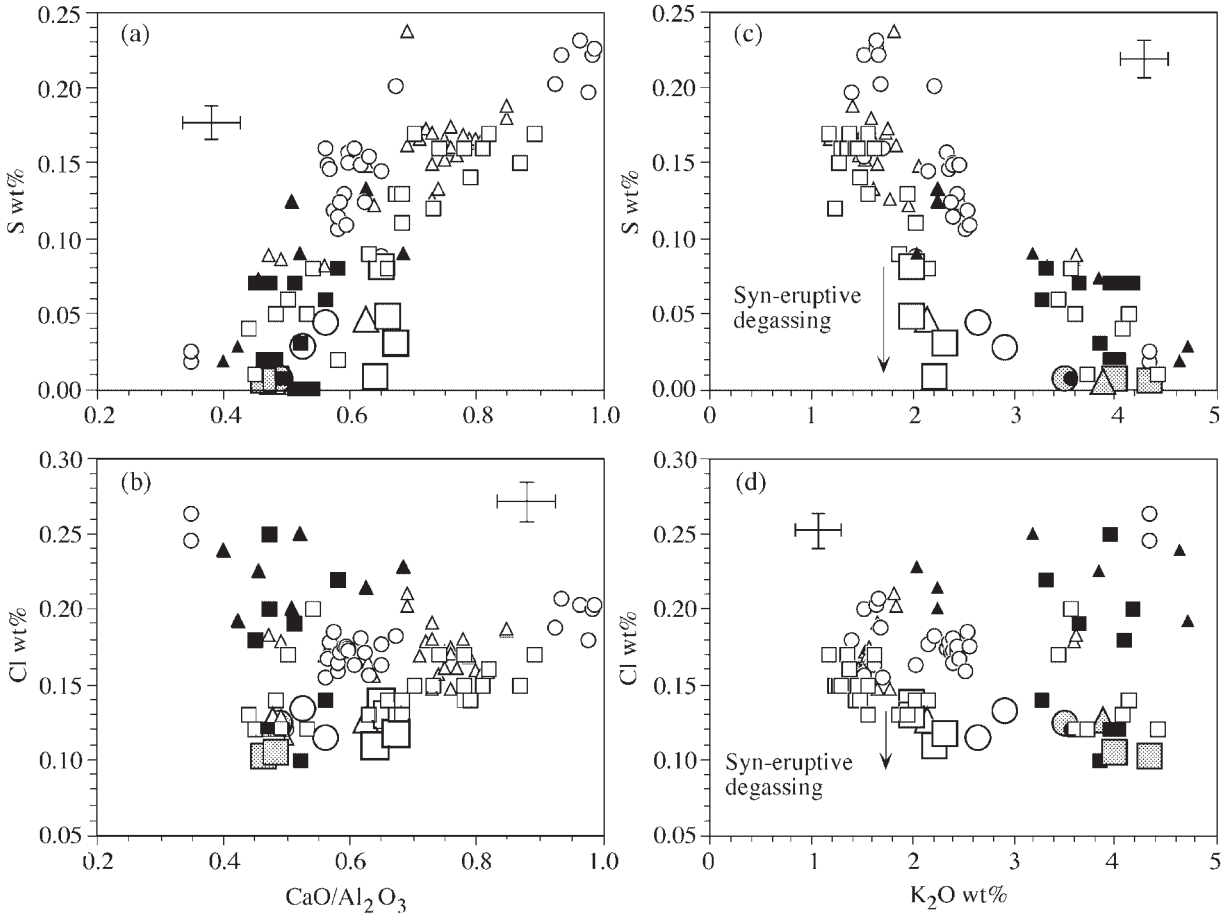

Fig. 8. Plots showing the sulphur and chlorine variations in MI and groundmass glasses as a function of CaO/Al_2O_3 ratio and K_2O content from the scoria–pumice pairs (ST130p, ST133s, ST82s/p, ST79 s/p). Symbols as in Fig. 6.

DISCUSSION

Melt inclusion study indicates that melts involved in the current activity of Stromboli cover a compositional range with CaO/Al_2O_3 = 0·99–0·29 and K_2O/Na_2O = 0·65–2·2, far wider than the compositional range of the magmas emitted during both normal Strombolian and more energetic explosions.

Volatile-rich magmas

In pumices, rare olivines $Fo_{88–89}$ have preserved volatile-rich primitive magma compositions as MI. They show high CaO/Al_2O_3 (>0·9) and high volatile concentrations with 1106 ppm CO_2 and 2·3 wt % H_2O. In terms of both major and volatile elements, these MI illustrate for the first time that volatile-rich and primitive mantle-derived melts rose, but either they never erupted or have not yet been identified.

Similarly, MI with CaO/Al_2O_3 ratio between 0·90 and 0·60 are characterized by high volatile contents (3·4 wt % of total volatiles). They contain up to 1689 ppm CO_2, 2·4–2·8 ± 0·3 wt % H_2O, 1660 ± 110 ppm S, 1660–1730 ± 100 ppm Cl and 680–640 ± 120 ppm F, with S/Cl and Cl/F ratios 0·95–1·0 and 2·4–2·7, respectively. These volatile concentrations are regarded as representative of the pre-eruptive H_2O, S, Cl and F contents of the crystal-poor magmas erupted during the current activity. Rather high volatile concentrations, particularly H_2O, in these melts in addition to low proportions of crystals contribute to lower both the viscosity and the density of the magma. The density at 1150°C is calculated to be 2500 kg/m^3 [following Lange (1994)] and viscosity close to 15–20 Pa/s [following Marsh (1989)] for magma blobs giving rise to pumice, with 10 vol. % crystals (Ol + Cpx + Plag) and 2·5 wt % H_2O.

Fractionation of clinopyroxene and olivine can account for the compositional variations between the volatile-rich

Table 4a: Water concentrations in melt inclusions and rim glasses of olivine from the scoriae

Sample	Fo[a] (mol %)	*e*[b] (μm)	*S*[c] (3535 cm^{-1})	Abs.	H_2O[d] (wt %)
St82s-oln1	72·7	48	0·66	0·080	0·17
St82s-oln2	72·7	55	0·66	0·082	0·15
St82s-oln3	72·7	56	0·66	0·087	0·16
St82s-ol3-rim	glass	56	0·66	0·087	0·16
St82s-oln4	72·8	32	0·66	0·057	0·18
St79s-ol n1	64·2	51	0·66	0·058	0·12
Reference glasses					
EtII-3[e] [3·5 wt %]		35	0·64	1·16	3·4
EtII-7[e] [1·5 wt %]		46	0·62	0·74	1·7

[a]Fo is the host olivine composition as [100 × Mg/(Mg + Fe)]. [b]Sample thickness. [c]S = [(Si + Al)/Σcations] ratio. [d]H_2O concentrations calculated with ε^{3535} (absorptivity coefficient) = 64·3 L/mol per cm (see text). [e]Reference glasses whose total H_2O concentrations, given in brackets, were determined by Karl–Fisher titration (CRSCM-CNRS, Orléans).

melts, particularly well illustrated by the range in the CaO/Al_2O_3 ratios. Plagioclase seems to play a minor role, as suggested by the constant K_2O/Na_2O ratio and the increase of Al_2O_3 content with decreasing CaO/Al_2O_3 ratio, although the light negative Eu anomaly in whole rocks (Fig. 3) attests to its fractionation. However, several processes may have been superimposed to account for the chemical variations observed. Mixing processes between rather primitive magmas variable in CaO/Al_2O_3 ratios (0·98–0·58) are clearly recorded within a single small grain ($Fo_{88–86·4}$) in sample (ST79p) and by the occurrence of a thin film of weakly differentiated melt (CaO/Al_2O_3 ratio ~0·75) less evolved than the whole rock, wrapping another crystal from the ST82p sample. These observations suggest ascent of weakly differentiated magmas and mixing between melts that suffered early olivine and Ca-rich pyroxene fractionation to various extents. At present, the most primitive magmas are recognized among the present products only on the microscopic scale of observation, possibly because of a low supply rate of magma.

Relationships between the crystal-poor and crystal-rich magmas (pumice–scoria pair)

Very different processes seem to control the petrogenetic relationships between crystal-poor and crystal-rich magmas emitted as pumices and scoriae. The bulk-rock compositions of pumice and scoriae fall in a narrow compositional range (CaO/Al_2O_3 ~0·69–0·52 and K_2O/Na_2O ~0·68–0·92) that overlaps that of the groundmass of the pumices (Fig. 10). There are no significant differences in their major and trace element compositions, although the crystal content (plagioclase, clinopyroxene and minor olivine) varies from ≤10 to ~50 vol. %. Accordingly, the groundmass and whole-rock compositions are similar in pumices whereas least-squares mass balance calculations indicate that the groundmass of the scoriae can be derived from the whole rocks by crystallizing ~55 wt % plagioclase, clinopyroxene and olivine (59:29:12). These results are in agreement with the modal analyses of the scoriae.

The main difference between the crystal-poor and crystal-rich magmas is their volatile content, particularly the concentration of H_2O, which varies from 2·8 wt % in MI from the crystal-poor magma to ≤0·2 wt % in MI from the crystal-rich magma. The pre-eruptive temperatures of magmas, deduced from optical thermometry, are estimated to be between 1140 and 1100 ± 15°C. Therefore, the crystal-rich magma appears to result from the low-pressure crystallization of volatile-rich magmas driven by H_2O exsolution during decompression, which implies both high density (2700 kg/m^3; following Lange, 1994) and viscosity ($1·4 \times 10^4$ Pa/s, following Marsh, 1989) for such a mush.

The most evolved melt components represented by MI with the lowest CaO/Al_2O_3 (0·29–0·35) and the highest K_2O/Na_2O (1·46–1·77) ratios are included in the most evolved mineral phases. They attest to the existence of highly differentiated, water-poor melts possibly associated with cumulate zones located on the margins of the reservoir or feeding conduits.

Multi-stage degassing

We demonstrate that crystallization is mainly driven by decompression, and that water becomes the dominant volatile constituent exsolved from the magma at low pressure, assuming that shoshonitic-type melt becomes saturated with respect to H_2O at nearly 80 MPa PH_2O, in a CO_2-free system (Métrich & Rutherford, 1998). Subsequently, water may act as the main carrier gas with respect to S and Cl. An attempt has been made to model the fractionation of S and Cl, during crystallization and exsolution of a H_2O-rich vapour phase, to account for the variability in S (from 1660 to ~800 ppm, Fig. 11a) and Cl (from 1660 to ~2400 ppm, Fig. 11b). Calculations are based on S, Cl and H_2O concentrations determined in olivine-hosted MI from scoria and pumice pairs (ST82s/p, ST133s/ST130p). The proportion of H_2O in the bulk assemblage (mineral phase + vapour) extracted during crystallization is evaluated on the basis of a

Table 4b: Water and carbon concentrations in melt inclusions of olivine from the pumices

Sample	Fo[a] (mol %)	X_{Fo}[a]	e[b] (μm)	Ca/Al[c]	N[d]	Abs. 1515 cm^{-1}	ε^{1515}	C (ppm)[e]	C_{cor} (ppm)[e]	CO_2 (ppm)
St82p-oln52a	84·6	0·05	100	0·73	0·269	0·251	359	312	296	1087
St82p-oln52a	84·6	0·05	100	0·73	0·269	0·238	359	296	281	1031
St82p-oln9b	84·6	0·09	42	0·85	0·226	0·178	374	506	461	1689
Average (n = 6)								(SD = 50)		
St82p-oln50	83·7	0·02	75	0·64	0·306	0·145	346	249	244	894
St82p-oln51	83·8	0·06	28	0·72	0·268	0·089	359	396	372	1365
St82p-oln51	83·8	0·06	28	0·72	0·268	0·083	359	367	345	1266
St79p-oln8	82·0	0·12	18	0·98	0·215	Interferences				
St79p-oln30	88·0	0·06	27	0·99	0·220	0·073	376	321	302	1107
Reference glass										
EtII-1[f]	[296 ppm]		84	0·62	0·397	0·309	315	301 (SD = 28)		

Sample	S[g]	Abs. 3535 cm^{-1}	H_2O[h] (wt %)	Abs. 5200 cm^{-1}	ε^{5200}	H_2O_{mol} (wt %)[i]	Abs. 4500 cm^{-1}	ε^{4500}	OH^-[i] (wt %)	H_2O_{total} (wt %)[j]
St82p-oln52a	0·67	Sat.	n.d.	0·016	0·81	1·3	0·014	0·64	1·5	2·7
St82p-oln52a	0·67	Sat.	n.d.	0·016	0·81	1·3	0·015	0·64	1·6	2·8
St82p-oln9b										
Average[k]	0·67	1·25	3·1							2·8
St82p-oln50	0·67	Sat.	n.d.	0·013	0·83	1·4	0·011	0·66	1·5	2·7
St82p-oln51	0·68	0·69	2·5							2·4
St82p-ol n51	0·68	0·69	2·5							2·4
St79p-oln8	0·62	0·45	2·6							2·3
St79p-oln30	0·65	0·64	2·4							2·3

[a]Fo and X_{Fo} are the host olivine composition as [100 × Mg/(Mg + Fe)] and the fraction of olivine post-entrapment crystallization, respectively. [b]Sample thickness. [c][CaO/Al_2O_3] wt ratio. [d][Na/(Na + Ca)]ratio. [e]C, concentrations calculated with absorptivity coefficient ε^{1515}; $C_{cor.}$, the concentration corrected for the post-entrapment crystallization of olivine (X_{Fo}). [f]Reference glasses whose C concentrations, in brackets, were determined by nuclear reaction analysis. [g][(Si + Al)/Σcations] ratio. [h]H_2O concentrations calculated with ε^{3535} (absorptivity coefficient) = 64·3 L/mol per cm (see text). [i]H_2O dissolved as molecular H_2O (H_2O_{mol}) and OH^- calculated with ε^{5200} and ε^{4500}, respectively (see text). [j]Total water concentrations corrected for the post-entrapment crystallization of olivine (X_{Fo}). [k]Average of six measurements. Sat., saturated; n.d., not determined; SD, standard deviation.

Rayleigh fractionation model $C_i = C_0 f^{D-1}$, where D is the bulk partition coefficient and f is the fraction of the remaining liquid. Potassium was considered as the index of differentiation. The model fits the data with $D_S^{fluid/melt} = 40$ (Fig. 11a) and $D_{Cl}^{fluid/melt} = 10$ (Fig. 11b). Similar partition coefficients between fluid and melt ($D_S = 34$ and $D_{Cl} = 2{\cdot}8$) were calculated with the same procedure on the basis of olivine-hosted MI from the Fuego 1974 eruption (Sisson & Layne, 1993).

The most evolved MI (3·5–4·5 wt % K_2O) recorded late but drastic depletion of S and Cl, whereas the magma becomes significantly depleted with respect to water (Fig. 11a and b). Sulphur decline may be related to its fractionation by a sulphide immiscible liquid together with variations in redox conditions in response to water loss and crystallization. But sulphides are uncommon except in MI from Fe-rich olivine interpreted as inherited from the cumulate zones developed on the margins of the conduits. In addition, the S content of scoriae as whole rock does not reach 100 ppm (Table 1). Thus, if S could be partly removed through sulphide globules, they might have been mobilized in vapour and in this case sulphide must be taken into account in the global sulphur budget. Desulphurization of magmatic sulphides resulting in Fe-oxide globules may occur in a wide range of rhyolitic to basaltic lavas and provide an efficient way to mobilize sulphur from immiscible sulphide globules during decompression and degassing processes (Larocque

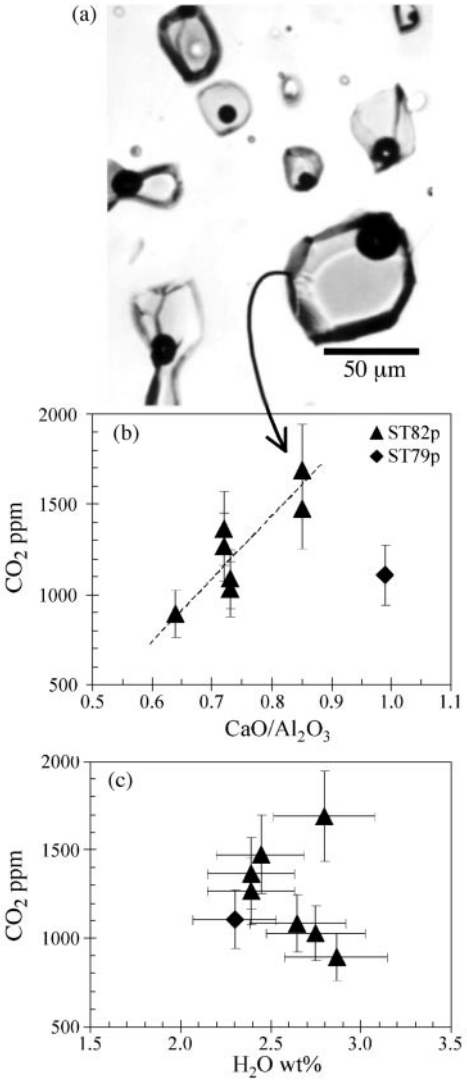

Fig. 9. (a) MI in olivine $Fo_{84\text{-}4}$ (sample ST82p, oln9, Table 2) containing glass with high CO_2 concentrations (1689 ppm CO_2, Table 4b) and one bubble with small carbonate crystals; plots of CO_2 vs CaO/Al_2O_3 ratio (b) and CO_2 vs H_2O (c) in MI hosted in olivine grains from the pumices.

Table 5: Optical thermometry measurements on melt inclusions in olivine

Sample	Fo[a]	T_m[b]	T_h[c]
Pumices			
St82p	86·9–87·4	1105	1140
St82p	81·5–82·1	1090*	n.d.
		1085*	n.d.
St82p	81·6–82·1	1090*	n.d.
		1090*	n.d.
St82p	80–81·8	1085	1125
Scoriae			
St82s	71·7–72·7	1090*	1101
		1085*	
St82s	72·3	1090	n.d.
St82s	71·7–72·7	1095	1125
St82s	72·3–72·7	1097*	1115
		1102*	

[a][100 × Mg/(Mg + Fe)]. [b]T_m, temperature of melting of the last nuclei. [c]T_h, temperature of homogenization (see text). *Duplicated measurements.

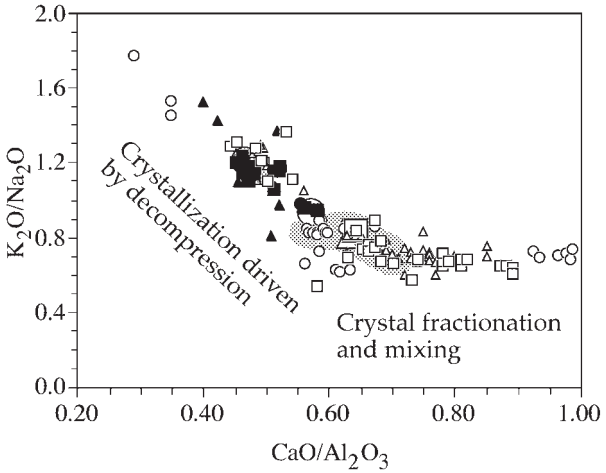

Fig. 10. Whole-rock compositions compared with glassy groundmass and MI compositions in CaO/Al_2O_3 vs K_2O/Na_2O diagram. The grey field represents the compositional range of whole rocks from trenches 1 and 2 and of the products emitted in the past 15 years including the 23 August 1998 explosion. Symbols as in Fig. 6.

et al., 2000). Conversely, efficient depletion in both S and Cl (Fig. 11) could support the idea of their fractionation in the vapour phase, with increasing partition coefficients ($D_S \gg 40$ to 100 and $D_{Cl} > 10$ to 30) and fraction of the vapour phase ($H_2O + CO_2$), in the uppermost part of the system (Fig. 11a and b). Increasing the proportions of the vapour phase agrees with a bubbling regime sustained by deep CO_2 flux (Allard *et al.*, 1994), and bubble accumulation at the base of the shallow pipes that connect the crack-like conduits to the surface (Jaupart & Vergniolle, 1988; Chouet *et al.*, 1997). This model, still poorly constrained, should imply time for diffusion between gas and melt and a rather large variability of the composition of the gas phase emitted at the craters, depending on the size of bubbles, their ascent rate and the energy of the eruption. Alternatively or in addition, mixing between an extensively degassed magma and magma blobs that differ in their volatile content may account for the variability observed. Such a model is

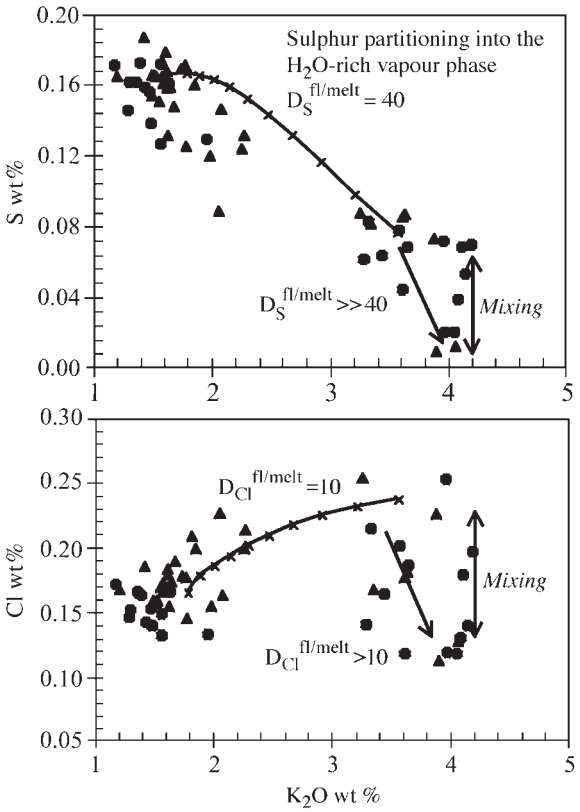

Fig. 11. Plots of S, Cl contents in MI and groundmass glasses from the samples St130p, St133s (23 August 1998 eruption) and St82s/p (last cycle of activity) vs their K_2O concentrations. The curves calculated for S and Cl are based on the Rayleigh fractionation model $C_i = C_0 f^{D-1}$, where D is the bulk partition coefficient ($\alpha D^{fl/melt} + \beta D^{solid}$), where α and β are the proportions of the fluid phase and of the solid, respectively; f is the fraction of residual melt calculated with K_2O; C_0 and C_i are the initial and final concentrations of element i, respectively. The fraction fluid (α) corresponds to H_2O exsolved from the magma. As the paragenesis is made of olivine + pyroxene + plagioclase, the term βD^{solid} is neglected. We have considered the initial conditions as C_0 = 1660 ppm for S and Cl, and 2·5 wt % H_2O; and final conditions with H_2O = 0·2 wt % and 4·6 wt % K_2O in melt, with 6·9 wt % H_2O released at the end.

consistent with very low pressure S loss ($\leq$20 MPa; Moore & Schilling, 1973) together with Cl, and passive degassing at the craters (Allard *et al.*, 1994). It is supported by the strong zoning of most of the phenocrysts of pumices, particularly well documented through the olivine grains, which attests to the recycling of crystals from the crystal-rich magma in the crystal-poor magma blobs at the origin of the highly vesicular pumices. Finally, we may expect that the extensively degassed magma (with respect to CO_2, H_2O, S, Cl and F to lesser extents), forming a viscous mush in the shallow pipes or possibly deeper, and sporadically disrupted and thrown away as lava lumps during 'normal' activity, contributes to the steady-state behaviour at Stromboli by capping the system.

Inference on (PCO_2 + PH_2O) fluid pressure and magma transfer

The CO_2 concentrations recorded in MI decline whereas their H_2O content increases (Fig. 9c). This trend is not consistent with a single process of open-system degassing, which should result in significant depletion in CO_2 but rather low H_2O variation (Dixon, 1997). Although there is a need for a larger dataset both on the natural MI, mainly obtained for a single sample (ST82p), and on experimental CO_2 solubility in shoshonitic melts, the point that arises is that the $P(CO_2 + H_2O)$ recorded in the MI (CO_2 = 1689–894 ppm and H_2O = 2·4–2·8 wt %) may possibly reach or exceed 350–400 MPa (Papale, 1999). High fluid pressures preserved in these MI, rather primitive in major element compositions, and hosted in small euhedral crystals ($\sim$500 μm in size) or crystals that are growing from a magma whose total content in crystals is a few per cent, strongly suggest a rapid ascent and short transfer of magma through the volcanic pile and eruption. This interpretation involves very rapid growth of olivine as has been hypothesized in the case of the Kilauea Iki 1959 eruption, for which 0·5–2 mm olivine grains were supposed to grow in <20 days (Wallace & Anderson, 1998).

CONCLUSIONS

The peculiar feature of Stromboli is its persistent activity, which has been fed by magmas differing chiefly in crystal and volatile contents, and whose characteristics have remained constant since the beginning of the present activity, about 1800–1400 years ago (Rosi *et al.*, 2000).

Magma with 50 vol. % crystals, rather homogeneous in major elements and degassed (nearly 0·2 wt % H_2O in the melt), constitutes a mush (Marsh, 1989) within the uppermost part of the plumbing system and probably sustains the current normal activity.

The violent explosions produce highly vesicular pumices in addition to crystal-rich scoriae, with virtually the same chemical composition, but with low-crystal (<10 vol. %) and high-volatile (up to 3·4 wt %) contents. The mineralogy and the chemistry of MI indicate crystallization out of equilibrium and mixing between crystal-poor magma batches that suffered variable extents of crystal fractionation. On the basis of the estimated total pressures (possibly 350–400 MPa) the volatile-rich magmas are deep seated.

We propose that these magmas contribute to the renewal of the crystal-rich magma body through decompression and water exsolution. Their crystallization induced by H_2O loss is accompanied by the release of S and Cl, water possibly acting as the main carrier gas.

Following this line of reasoning, the CO_2- and H_2O-rich magma blobs periodically or continuously refill the

shallow part of the volcano, and partially mingle with the crystal-rich body. The strong zoning of most of the phenocrysts of pumices, particularly well documented through the olivine crystals, indicates that crystals from the crystal-rich magma were recycled in the crystal-poor magma blobs at the origin of the highly vesicular pumices. Time was sufficient to allow crystallization of broad intermediate zones of a few tenths of a micrometre, strongly heterogeneous in composition ($Fo_{73–80}$) and surrounding strongly resorbed Fe-rich cores. In addition, we expect that the resorbed Fe-rich cores act as nuclei that have helped the olivine growth during magma ascent.

Given the very limited compositional range between scoriae and pumices, the volume of the volatile-rich magmas that have fed the shallow system could, on average, match that of the magma withdrawn during the normal Strombolian activity and lava flow episodes. However, this is not consistent with the degassing budget at Stromboli (Allard *et al.*, 1994).

We have no data with which to model precisely the interface between the two magmas; however, the crystal-rich body displays high density (2700 kg/m^3) and viscosity ($1{\cdot}4 \times 10^4$ Pa/s), whereas the crystal-poor magma batches have very low density (2500 kg/m^3) and viscosity (15–20 Pa/s). The density contrast makes the system gravitationally unstable and prevents the development of stratified layers with a large interface. It is likely that the density contrast induces overturns (Cardoso & Woods, 1999), which may promote mechanical mixing between the two magmas. In addition, the strong viscosity contrast could facilitate the formation of plumes of crystal-poor magmas with highly vesicular heads, which swell and accelerate as they rise (Thomas *et al.*, 1993). In this interpretation the emission of the volatile-rich magma batches, resulting in pumice, is explained by rapid decompression and almost instantaneous H_2O and CO_2 release (Proussevitch & Sahagian, 1998).

It is worth noting that there is a continuous increase in the energy released between the 'normal' activity with gas jets and scoriae expulsion and the violent explosions with discharge of volatile-rich magma blobs. As a result, we expect that the uprising and degassing of water-rich magma pockets, when this magma is not emitted, contributes to the major explosions with a high proportion of gas release.

ACKNOWLEDGEMENTS

We thank C. Cashman, J. Barclay and C. Mandeville for their careful reviews, M. Wilson for her constructive suggestions, P. Papale for having calculated the fluid pressures and for fruitful discussions, B. Scaillet for having provided the H_2O-rich reference glasses, and F. Colarieti and E. S. Waguena for assistance during the sample preparation. This work was supported by Gruppo Nazionale per la Vulcanologia (CNR), Italy, and CEE-program ENV4-CT-96–0259.

REFERENCES

Allard, P., Carbonelle, J., Métrich, N., Loyer, H. & Zettwoog, P. (1994). Sulphur output and magma degassing budget of Stromboli volcano. *Nature* **368**, 326–330.

Barberi, F., Rosi, M. & Sodi, A. (1993). Volcanic hazard assessment at Stromboli based on review of historical data. *Acta Vulcanologica* **3**, 173–187.

Bertagnini, A., Coltelli, M., Landi, P., Pompilio, M., & Rosi, M. (1999). Violent explosions yield new insights into dynamics of Stromboli volcano. *EOS Transactions, American Geophysical Union* **80**(52), 633–636.

Bonaccorso, A., Cardaci, C., Coltelli, M., Del Carlo, P., Falsaperla, S., Panucci, S., Pompilio, M. & Villari, L. (1996). Annual report of the world volcanic eruptions in 1993, Stromboli. *Bulletin of Volcanic Eruptions* **35**, *Supplement*, 8–14.

Cardoso, S. S. S. & Woods, A. W. (1999). On convection in a volatile-saturated magma. *Earth and Planetary Science Letters* **168**, 301–310.

Chouet, B., Hamisevicz, N. & McGetchin, T. R. (1974). Photoballistics of volcanic jet activity at Stromboli, Italy. *Journal of Geophysical Research* **79**, 4961–4976.

Chouet, B., Saccorotti, G., Martini, M., Dawson, P., De Luca, G., Milana, G. & Scarpa, R. (1997). Source and path effects in the wave fields of tremor and explosions at Stromboli volcano, Italy. *Journal of Geophysical Research* **102**, 15129–15150.

Coltelli, M., Falsaperla, S., Del Carlo, P., Pompilio, M. & Bonaccorso, A. (1999). Volcanic, seismic, and ground deformation data concerning the Stromboli volcano in 1995. *Bulletin of Volcanic Eruptions* **35**, *Supplement*, 8–14.

Dixon, J. E. (1997). Degassing of alkalic basalts. *American Mineralogist* **82**, 368–378.

Dixon, J. E. & Pan, V. (1995). Determination of the molar absorptivity of dissolved carbonate in basaltic glass. *American Mineralogist* **80**, 1339–1342.

Dixon, J. E., Stolper, E. M. & Holloway, J. R. (1995). An experimental study of water and carbon dioxide solubilities in mid-ocean ridge basaltic liquids. Part I: calibration and solubility models. *Journal of Petrology* **36**, 1607–1631.

Francalanci, L., Tommasini, S., Conticelli, S. & Davies, G. R. (1999). Sr isotope evidence for short magma residence time for the 20th century at Stromboli volcano, Italy. *Earth and Planetary Science Letters* **167**, 61–69.

Giberti, G., Jaupart, C. & Sartoris, G. (1992). Steady-state operation of Stromboli volcano, Italy: constraints on the feeding system. *Bulletin of Volcanology* **54**, 535–541.

Horning-Kjarsgaard, I., Keller, J., Koberski, U., Stadlbauer, E., Francalanci, L., & Lenhart, R. (1993). Geology, stratigraphy and volcanological evolution of the island of Stromboli, Aeolian arc, Italy. *Acta Vulcanologica* **3**, 21–68.

Jaupart, C. & Vergniolle, S. (1988). Laboratory models of Hawaiian and Strombolian eruptions. *Nature* **331**, 58–60.

Kokelaar, P. & Romagnoli, C. (1995). Sector collapse, sedimentation and clast population evolution at an active island-arc volcano: Stromboli, Italy. *Bulletin of Volcanology* **57**, 240–262.

Lange, R. A. (1994). The effect of H_2O, CO_2 and F on the density and viscosity of silicate melts. In: Carroll, M. R. & Holloway, J. R. (eds) *Volatile in Magmas. Mineralogical Society of America, Reviews in Mineralogy* **30**, 331–370.

Larocque, A. C. L., Stimac, J. A., Keith, J. D. & Huminicki, M. A. E. (2000). Destabilization of immiscible sulfides in silicate melts: implications for the contribution of metals and sulfur to magmatic ore-forming fluids. *IAVCEI General Assembly*, 18–22 July, Bali, p. 120 (abstract).

Marsh, B. D. (1981). On the crystallinity, probability of occurrence, and rheology of lava and magma. *Contributions to Mineralogy and Petrology* **78**, 85–98.

Marsh, B. D. (1989). Magma chamber. *Annual Review of Earth and Planetary Sciences* **17**, 439–474.

McDonough, W. F. & Sun, S. (1995). The composition of the Earth. *Chemical Geology* **120**, 223–253.

Métrich, N. & Clocchiatti, R. (1996). Sulphur abundance and its speciation in oxidized alkaline melts. *Geochimica et Cosmochimica Acta* **60**, 4151–4160.

Métrich, N. & Mosbah, M. (1988). Détermination des teneurs en carbone de quelques verres basaltiques; analyses par réactions nucléaire. *Bulletin de Minéralogie* **111**, 511–522.

Métrich, N. & Rutherford, M. J. (1998). Low pressure crystallization paths of H_2O-saturated basaltic–hawaiitic melts from Mt Etna: implications for open-system degassing volcanoes. *Geochimica et Cosmochimica Acta* **62**, 1195–1205.

Moore, J. G. & Schilling, J. G. (1973). Vesicles, water and sulfur in Reykjanes ridge basalts. *Contributions to Mineralogy and Petrology* **28**, 272–279.

Mosbah, M., Métrich, N. & Massiot, P. (1991). PIGME fluorine determination using a nuclear microprobe with application to glass inclusions. *Nuclear Instruments and Methods in Physics Research* **B58**, 227–231.

Pandya, N., Muenow, D. W. & Sharma, S. K. (1992). The effect of bulk composition on the speciation of water in submarine volcanic glasses. *Geochimica et Cosmochimica Acta* **56**, 1875–1883.

Papale, P. (1999). Modeling of the solubility of two-component H_2O–CO_2 fluid in silicate liquids. *American Mineralogist* **84**, 477–492.

Pasquaré, G., Francalanci, L., Garduño, V. H. & Tibaldi, A. (1993). Structure and geologic evolution of the Stromboli volcano, Aeolian Islands, Italy. *Acta Vulcanologica* **3**, 79–89.

Pasteris, J. D. (1987). Fluid inclusions in mantle xenoliths. In: Nixon, P. H. (ed.) *Mantle Xenoliths*. Chichester: Wiley, pp. 692–707.

Peccerillo, A. & Taylor, S. R. (1976). Geochemistry of Eocene calc-alkaline volcanic rocks from Kastamonu area, northern Turkey. *Contributions to Mineralogy and Petrology* **58**, 63–81.

Perret, F. A. (1913). Report on the recent great eruption of the volcano Stromboli. *Smithsonian Report* **1912**, 285–289.

Proussevitch, A. A. & Sahagian, D. L. (1998). Dynamics and energetics of bubble growth in magmas. Analytical formulation and numerical modeling. *Journal of Geophysical Research* **103**(B8), 18223–18251.

Ripepe, M., Rossi, M. & Saccorotti, G. (1993). Image processing of explosive activity at Stromboli. *Journal of Volcanology and Geothermal Research* **54**, 335–351.

Ripepe, M., Poggi, P., Braun, T. & Gordeev, E. (1996). Infrasonic waves and volcanic tremor at Stromboli. *Geophysical Research Letters* **23**, 181–184.

Roedder, E. (1984). Inclusion measurements: heating, cooling, decrepitation and crushing. In: Roedder, E. (ed.) *Fluid Inclusions. Mineralogical Society of America, Reviews in Mineralogy* **12**, 181–221.

Rosi, M., Bertagnini, A. & Landi, P. (2000). Onset of the persistent activity at Stromboli volcano (Italy). *Bulletin of Volcanology* **62**, 294–300.

Sisson, T. W. & Layne, G. D. (1993). H_2O in basalt and basaltic andesite glass inclusions from 4 subduction-related volcanoes. *Earth and Planetary Science Letters* **117**, 619–635.

Sobolev, A. V., Dmitriev, L. V., Barsukov, Nevsorov, V. N. & Slutskiy, A. B. (1980). The formation conditions of high magnesian olivines from the monomineral fraction of Luna-24 regolith. *Proceedings of the 11th Lunar and Planetary Science Conference*, pp. 105–106.

Thomas, N., Tait, S. & Koyaguchi, T. (1993). Mixing of stratified liquids by the motion of gas bubbles: application to magma mixing. *Earth and Planetary Science Letters* **115**, 505–516.

Thordarson, T., Self, S., Oskarsson, N. & Hulsechosch, T. (1996). Sulfur, chlorine and fluorine degassing and atmospheric loading by the 1783–1784 AD (Skaftar Fires) eruption in Iceland. *Bulletin of Volcanology* **58**, 205–225.

Vergniolle, S., Brandeis, G. & Mareschal, J.-C. (1996). Strombolian explosions. 2. Eruption dynamics determined from acoustic measurements. *Journal of Geophysical Research* **101**(B9), 20449–20466.

Wallace, P. & Anderson, J. R. (1998). Effects of eruption and lava drainback on the H_2O contents of basaltic magmas at Kilauea volcano. *Bulletin of Volcanology* **59**, 327–344.